Partial-Wave Analysis of $K^-p \to \pi^\pm\Sigma^\mp$ Between 1.73 and 2.11 GeV*

Daniel F. Kane, Jr.
Lawrence Berkeley Laboratory, University of California, Berkeley, California 94720
(Received 16 September 1971)

Cross-section, angular-distribution, and polarization measurements are presented for 17 energies. Results of a partial-wave analysis based on these data are presented. The presence of resonant structures in the F_{15} and D_{13} waves is confirmed. The masses, widths, and resonant amplitudes are determined: $E_R = 1.925 \pm 0.008$ GeV, $t = -0.137 \pm 0.015$, and $\Gamma = 0.146 \pm 0.022$ GeV for the F_{15}; $E_R = 1.985 \pm 0.005$ GeV, $t = -0.093 \pm 0.006$, $\Gamma = 0.208 \pm 0.022$ GeV for the D_{13}. The D_5 and F_5 octets, F_7 decuplet, and G_7 singlet are studied for SU_3 symmetry of reduced coupling constants; possible conclusions are limited by uncertainty about the detailed energy dependence of the couplings. The D_{13} resonance is shown to be compatible with the D_3 nucleon resonance seen around 2.040 GeV.

I. INTRODUCTION

We have studied the reactions $K^-p \to \pi^\pm\Sigma^\mp$ in the center-of-mass energy range 1.73–2.11 GeV. The data were obtained in two separate exposures, using the 25-in. hydrogen bubble chamber at the Lawrence Berkeley Laboratory, Berkeley.[1,2] The following discussion proceeds from the directly observed to the model-dependent interpretation. Section II describes how the data were brought into usable form. Section III presents the direct experimental results. Section IV exploits well-established properties of the strong interaction to represent the results in a generally useful form – the partial waves. Finally, Sec. V attempts to interpret these results in terms of the SU_3 symmetry model. Further details, both on the procedures of data reduction and about individual solutions of the partial-wave analysis, are presented in Ref. 2.

II. EXPERIMENTAL DETAILS

A. Normalization

Preliminary results of the first exposure have been presented,[3] but the cross sections disagreed with those obtained in another experiment.[4] We have renormalized these data, as described in Ref. 1, based on a high-statistics beam count. (We also reweighted events on an individual basis as described below.) The normalization for the second exposure was based on the τ-decay mode ($K^- \to \pi^-\pi^+\pi^-$). The results are shown in Table I; the momentum spread is due both to the momentum bite of the beam optics and to the ionization energy loss as the beam traversed the chamber. The mean momentum quoted was determined from the distribution of events passing cuts in beam phase space and chamber fiducial volume. These distributions are shown in Fig. 1. For the first exposure, fitted beam momenta from Σ events were used; for the second exposure, the fitted momenta of the τ decays were used.

B. Data Reduction

The film was scanned separately for events with kinking tracks (for the second exposure, the 3-prong topology was sought in the same scan). About 10% of the first exposure and 50% of the second were scanned a second time to determine the scanning efficiency. This varied from 92% to 97% for a single scan and was 99% for those momenta scanned completely twice.

The events were measured on the COBWEB system of on-line Franckensteins.[5] Geometrical reconstruction, kinematic fitting, and logical selection of events were performed on the FOG–CLOUDY-FAIR system of programs.[6] The kinematic fitting proceeded as follows. Whenever $\Delta p/p$ (measured) for the connecting track was >0.5, the fitting was first constrained at the decay vertex to determine the momentum of the connecting track. Since this was a zero-constraint fit, it in general gave two starting values for the subsequent two-vertex fit. Also for the Σ^+ events there were two decay modes: π^+n and π^0p. The following production vertex reactions were attempted:

$$K^-p \to \pi^\pm\Sigma^\mp$$
$$\to \pi^\pm\Sigma^\mp\pi^0$$
$$\to K^+\Xi^-.$$

Events that failed in geometrical reconstruction, or failed to fit any two-vertex kinematic hypothesis with a reasonable χ^2, or that fit more than one hypothesis well became candidates for remeasure. Events with a well-measured connecting track indicative of a long lifetime were assumed to be meson $(\pi^\pm, K^-)$ decays and were eliminated from

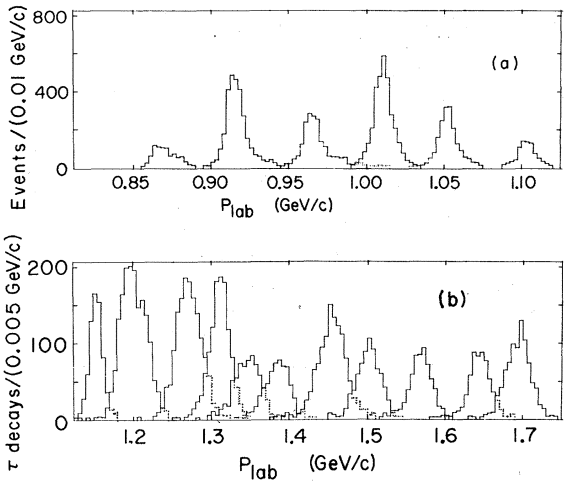

FIG. 1. Distribution of fitted momenta: (a) From exposure described in Ref. 1 (fitted momenta of Σ events). (b) From exposure described in Ref. 2 (fitted momenta of τ decays).

the remeasure sample (a lifetime cut and reweighting procedure accounted for any good events lost by this). An ionization scan was carried out for events fitting more than one hypothesis; events whose ambiguities could be so resolved were also eliminated from the remeasure sample. The events that were remeasured went through FOG-CLOUDY-FAIR and an ionization scan.

There still remained events that failed at some stage of the data reduction but that looked reasonable on the scan table. For the first exposure there were also some bookkeeping losses. These losses were taken into account in the determination of cross sections.

TABLE I. Beam normalizations.

Center-of-mass energy (GeV)	Lab momentum (GeV/c) $P \pm \Delta P$	Events/mb
1.732	0.870 ± 0.025	378 ± 20
1.754	0.917 ± 0.016	1280 ± 79
1.782	0.975 ± 0.026	1241 ± 72
1.798	1.010 ± 0.013	1549 ± 84
1.818	1.053 ± 0.013	831 ± 42
1.844	1.109 ± 0.014	325 ± 23
1.865	1.153 ± 0.011	435 ± 18
1.887	1.201 ± 0.022	1102 ± 32
1.919	1.271 ± 0.021	1068 ± 32
1.937	1.310 ± 0.017	866 ± 27
1.952	1.345 ± 0.020	515 ± 23
1.970	1.384 ± 0.018	489 ± 22
2.001	1.454 ± 0.023	935 ± 34
2.022	1.500 ± 0.020	617 ± 25
2.051	1.567 ± 0.019	537 ± 24
2.084	1.644 ± 0.017	551 ± 25
2.106	1.694 ± 0.019	804 ± 32

The scan for kinking tracks missed two classes of Σ events: those for which the decay occurred too close to the production vertex or outside the chamber and those with imperceptible kinks. These losses are related to the lifetime and decay angular distributions and can be corrected without biasing the study of the production reaction. The natures of these distributions are known; for a given set of cuts in the length of track and decay angles, each event can be weighted by the inverse of the fraction of the distributions passing these acceptance criteria. As the cuts are increased, a point is reached where the increase in weights just compensates for the events newly rejected; the weighted number of events ceases to change (within statistical limits). By this method we found the appropriate cuts for use in determining the cross sections.

In accepting events for angular distributions, where absolute numbers of events were not critical, the cuts were relaxed where losses were uncorrelated with the production angle. This primarily involved elimination of the cut in the azimuthal decay angle: For decays toward or away from the cameras, resulting in a small apparent kink, there was about 35% loss of events. The affected portions of this distribution were eliminated when determining the cross sections, but these events were used in the angular distributions. The events of the type $\Sigma^+ \to \pi^0 p$ were used only to obtain polarizations; for this measurement each bin of the angular distribution is treated separately – even relative numbers of events from one bin to another are not critical. The cuts used in this last case were minimal, and the events were used unweighted. Finally, the cuts made in the beam phase space for events used in angular distributions and polarizations were slightly less stringent than those used in cross-section determinations.

The distributions of lifetimes were found to be exponential, as expected, except for losses due to very short tracks and decays outside the chamber. We determined the mean lifetimes for events passing all (angular distribution type) cuts, using a maximum-likelihood technique. These mean lifetimes for the various decay types are (in nsec): 0.153 ± 0.005 for $\Sigma^- \to \pi^- n$, 0.091 ± 0.004 for $\Sigma^+ \to \pi^0 p$, and 0.085 ± 0.003 for $\Sigma^+ \to \pi^+ n$.

III. EXPERIMENTAL RESULTS

A. Cross Sections

The details and results of the cross-section determinations are presented in Table II. We have plotted these results in Fig. 2, along with the data available in the literature.[4,7] The results from our

TABLE II. Cross sections.

$E_{c.m.}$ (GeV)	$K^-p \to \pi^+\Sigma^-$ Number unweighted	Mean weight	$\sigma \pm \Delta\sigma$ (mb)	$K^-p \to \pi^-\Sigma^+$ Number unweighted	Mean [a] weight	$\sigma \pm \Delta\sigma$ (mb)
1.732	169	2.14	1.17 ± 0.14	101	2.40	1.66 ± 0.23
1.754	547	2.10	1.07 ± 0.12	374	2.40	1.76 ± 0.20
1.782	431	2.13	1.01 ± 0.11	268	2.38	1.48 ± 0.17
1.798	678	2.15	1.15 ± 0.12	457	2.35	1.80 ± 0.19
1.818	400	2.19	1.29 ± 0.14	220	2.43	1.67 ± 0.19
1.844	174	2.18	1.44 ± 0.19	74	2.51	1.50 ± 0.24
1.865	274	1.62	1.08 ± 0.09	119	2.21	1.36 ± 0.14
1.887	517	1.64	0.83 ± 0.05	324	2.10	1.42 ± 0.10
1.919	325	1.64	0.54 ± 0.04	310	2.16	1.42 ± 0.10
1.937	226	1.66	0.46 ± 0.04	246	2.00	1.28 ± 0.10
1.952	101	1.67	0.36 ± 0.04	137	2.09	1.29 ± 0.13
1.970	95	1.72	0.35 ± 0.04	139	2.05	1.29 ± 0.13
2.001	208	1.70	0.40 ± 0.03	237	2.08	1.20 ± 0.10
2.022	118	1.70	0.36 ± 0.04	147	2.14	1.18 ± 0.11
2.051	97	1.74	0.34 ± 0.04	128	2.22	1.20 ± 0.12
2.084	94	1.73	0.33 ± 0.04	137	2.21	1.30 ± 0.13
2.106	121	1.74	0.29 ± 0.03	168	2.09	1.04 ± 0.10

[a] Does not include the factor due to decay branching fraction: 1/0.472.

experiment are in good agreement with the results of other experiments except in the case of the $\pi^+\Sigma^-$ final state in the resonance region around 1.85 GeV. We understand that new data will soon be available in this region.[8]

B. Angular Distributions

We have found the distribution of events in the production cosine, $\cos\theta = \hat{k}_K \cdot \hat{k}_\pi$, where $\hat{k}$ is the direction of the particle's momentum in the overall center-of-mass system. In Tables III and IV we present both the weighted and the unweighted numbers of events in 20 equal bins of $\cos\theta$. Because of limited statistics we believe that this form of presentation best preserves the information content of the experiment. When we used the data for analysis, we grouped bins by an algorithm that tended to preserve structure while increasing the statistical reliability of assigned errors.[2]

C. Polarizations

Since the Σ decay is parity-violating, the angular distribution of the decay particles in the Σ rest frame takes the form

$$f(\theta, \cos\chi)\, d\cos\chi = A[1 + \alpha P(\theta)\cos\chi]\, d\cos\chi,$$

where χ is the polar angle between the hyperon spin and the baryon decay directions, A and α are constants. The polarization, P, may depend on the production angle θ. We have observed such a decay assymetry for the type $\Sigma^+ \to \pi^0 p$, for which $\alpha \approx -1.0$; for the decays $\Sigma^\pm \to \pi^\pm n$, the values of α are approximately zero and our observations were consistent with this. We have used $\cos\chi = \hat{k}_p \cdot \hat{n}$, where $\hat{k}_p$ is the direction of the decay proton in the Σ rest frame. The production normal

$$\hat{n} = \frac{\hat{k}_K \times \hat{k}_\pi}{|\hat{k}_K \times \hat{k}_\pi|}$$

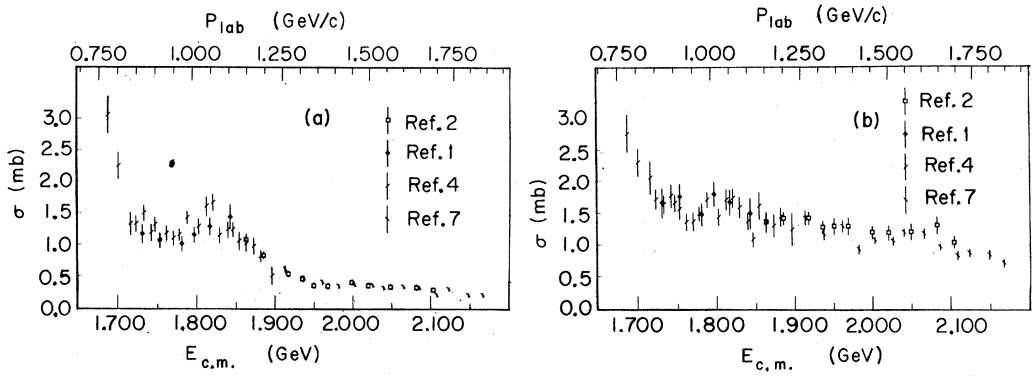

FIG. 2. Cross sections from all available data for the reactions studied. (a) $K^-p \to \pi^+\Sigma^-$. (b) $K^-p \to \pi^-\Sigma^+$.

TABLE III. $K^-p \to \pi^+\Sigma^-$ data binned in production cosine.

Center	1.732 GeV	1.754 GeV	1.782 GeV	1.798 GeV	1.818 GeV	1.844 GeV	1.865 GeV	1.887 GeV	1.919 GeV
	Number weighted/Number unweighted								
−0.95	19.7/ 15	95.1/ 71	44.7/ 33	63.1/ 46	45.9/ 33	18.4/ 13	32.7/ 28	60.0/ 51	37.9/ 32
−0.85	33.9/ 26	100.6/ 76	103.3/ 77	152.3/112	93.6/ 68	33.6/ 24	32.7/ 28	48.9/ 42	26.7/ 23
−0.75	36.2/ 28	123.0/ 94	118.4/ 89	165.5/123	89.8/ 66	29.1/ 21	41.7/ 36	32.6/ 28	14.1/ 12
−0.65	32.1/ 25	106.3/ 82	85.5/ 65	111.6/ 84	72.9/ 54	31.4/ 23	32.2/ 28	38.4/ 33	17.6/ 15
−0.55	10.2/ 8	79.7/ 62	66.5/ 51	105.3/ 80	50.5/ 38	18.9/ 14	18.5/ 16	26.6/ 23	15.2/ 13
−0.45	23.9/ 19	62.4/ 49	37.3/ 29	70.2/ 54	27.6/ 21	17.3/ 13	19.3/ 17	20.7/ 18	21.8/ 19
−0.35	12.6/ 10	37.8/ 30	38.3/ 30	42.4/ 33	19.5/ 15	5.3/ 4	6.8/ 6	10.3/ 9	5.8/ 5
−0.25	6.2/ 5	35.0/ 28	30.3/ 24	16.6/ 13	7.7/ 6	3.9/ 3	2.3/ 2	7.9/ 7	7.9/ 7
−0.15	1.2/ 1	26.0/ 21	13.8/ 11	29.0/ 23	14.0/ 11	6.4/ 5	4.6/ 4	6.8/ 6	9.0/ 8
−0.05	2.4/ 2	22.1/ 18	26.0/ 21	24.9/ 20	17.5/ 14	5.1/ 4	9.1/ 8	14.9/ 13	14.8/ 13
+0.05	8.5/ 7	26.8/ 22	31.9/ 26	38.3/ 31	21.1/ 17	7.5/ 6	10.3/ 9	21.8/ 19	17.3/ 15
+0.15	6.1/ 5	31.5/ 26	23.2/ 19	51.4/ 42	17.2/ 14	13.6/ 11	12.6/ 11	37.8/ 33	27.6/ 24
+0.25	14.5/ 12	34.9/ 29	21.8/ 18	64.3/ 53	35.3/ 29	24.5/ 20	25.4/ 22	57.8/ 50	27.6/ 24
+0.35	8.4/ 7	46.8/ 39	24.1/ 20	37.3/ 31	26.6/ 22	20.6/ 17	30.3/ 26	46.7/ 40	33.5/ 29
+0.45	15.7/ 13	34.8/ 29	21.6/ 18	37.3/ 31	31.2/ 26	15.6/ 13	19.9/ 17	55.1/ 47	31.4/ 27
+0.55	15.9/ 13	25.5/ 21	13.3/ 11	22.9/ 19	26.4/ 22	13.2/ 11	19.0/ 16	44.9/ 38	30.6/ 26
+0.65	12.5/ 10	22.3/ 18	11.1/ 9	13.5/ 11	11.0/ 9	10.9/ 9	18.1/ 15	49.3/ 41	13.2/ 11
+0.75	12.9/ 10	35.7/ 28	11.4/ 9	22.7/ 18	18.8/ 15	9.9/ 8	11.2/ 9	37.0/ 30	24.4/ 20
+0.85	31.2/ 23	43.9/ 33	33.5/ 25	82.1/ 62	39.3/ 30	28.6/ 22	36.3/ 28	75.6/ 59	31.9/ 25
+0.95	24.8/ 16	70.2/ 46	68.4/ 46	131.7/ 89	110.5/ 75	47.5/ 33	63.3/ 44	139.4/ 96	101.9/ 72
Total	328.8/255	1060.4/822	824.5/631	1282.2/975	776.4/585	361.1/274	446.5/370	832.5/683	510.3/420

Center	1.937 GeV	1.952 GeV	1.970 GeV	2.001 GeV	2.022 GeV	2.051 GeV	2.084 GeV	2.106 GeV
	Number weighted/Number unweighted							
−0.95	53.3/ 45	14.6/ 12	23.8/ 20	58.0/ 47	29.7/ 24	27.5/ 22	30.1/ 24	35.8/ 28
−0.85	19.3/ 16	7.0/ 6	14.3/ 12	24.3/ 19	26.8/ 21	18.3/ 14	9.7/ 8	19.1/ 15
−0.75	12.9/ 11	3.5/ 3	4.7/ 4	15.6/ 13	10.7/ 9	10.8/ 9	12.4/ 10	8.8/ 7
−0.65	9.2/ 8	4.6/ 4	3.5/ 3	11.3/ 9	11.1/ 9	9.0/ 7	3.7/ 3	4.0/ 3
−0.55	5.7/ 5	4.6/ 4	3.6/ 3	6.9/ 6	3.5/ 3	2.4/ 2	0 / 0	0 / 0
−0.45	5.7/ 5	3.4/ 3	4.6/ 4	9.4/ 8	3.5/ 3	3.5/ 3	4.7/ 4	3.9/ 3
−0.35	11.4/ 10	3.4/ 3	4.6/ 4	10.4/ 9	8.4/ 7	1.2/ 1	1.2/ 1	6.1/ 5
−0.25	9.0/ 8	4.5/ 4	0 / 0	8.1/ 7	6.0/ 5	1.1/ 1	1.2/ 1	4.6/ 4
−0.15	9.1/ 8	3.4/ 3	1.2/ 1	4.5/ 4	11.6/ 10	2.3/ 2	0 / 0	2.4/ 2
−0.05	4.6/ 4	3.4/ 3	1.1/ 1	2.3/ 2	2.3/ 2	1.2/ 1	1.2/ 1	2.3/ 2
+0.05	12.5/ 11	2.3/ 2	2.3/ 2	2.3/ 2	0 / 0	0 / 0	1.1/ 1	0 / 0
+0.15	13.7/ 12	6.8/ 6	1.1/ 1	2.5/ 2	0 / 0	1.1/ 1	2.3/ 2	3.4/ 3
+0.25	9.2/ 8	4.6/ 4	0 / 0	4.6/ 4	2.3/ 2	1.1/ 1	0 / 0	0 / 0
+0.35	18.4/ 16	4.6/ 4	10.4/ 9	5.7/ 5	5.8/ 5	1.2/ 1	2.3/ 2	1.1/ 1
+0.45	17.4/ 15	7.0/ 6	2.4/ 2	8.1/ 7	9.4/ 8	11.1/ 9	2.3/ 2	1.1/ 1
+0.55	16.4/ 14	5.9/ 5	1.2/ 1	3.5/ 3	3.5/ 3	2.3/ 2	4.6/ 4	5.8/ 5
+0.65	10.7/ 9	3.6/ 3	3.5/ 3	8.3/ 7	2.3/ 2	4.7/ 4	1.2/ 1	2.4/ 2
+0.75	9.7/ 8	11.0/ 9	6.1/ 5	8.5/ 7	4.8/ 4	3.6/ 3	3.6/ 3	4.7/ 4
+0.85	35.5/ 28	18.9/ 15	15.1/ 12	37.5/ 30	13.8/ 11	17.5/ 14	21.2/ 17	22.3/ 18
+0.95	89.0/ 63	45.1/ 32	63.6/ 45	98.5/ 70	63.5/ 45	64.6/ 46	52.2/ 38	67.5/ 49
Total	372.6/304	162.2/131	166.9/132	330.4/261	219.0/173	184.5/143	154.9/122	195.4/152

TABLE IV. $K^-p \to \pi^-\Sigma^+$ data binned in production cosine.

Center	1.732 GeV	1.754 GeV	1.782 GeV	1.798 GeV	1.818 GeV	1.844 GeV	1.865 GeV	1.887 GeV	1.919 GeV
	Number weighted/Number unweighted								
−0.95	12.1/ 10	42.3/ 35	35.1/ 29	43.7/ 36	29.2/ 24	4.9/ 4	11.6/ 10	45.3/ 39	41.2/ 35
−0.85	12.1/ 10	26.5/ 22	27.8/ 23	44.8/ 37	29.1/ 24	18.3/ 15	19.8/ 17	48.9/ 42	39.4/ 34
−0.75	15.7/ 13	39.8/ 33	27.8/ 23	47.2/ 39	31.5/ 26	4.9/ 4	9.3/ 8	18.7/ 16	30.3/ 26
−0.65	6.0/ 5	25.3/ 21	26.5/ 22	37.4/ 31	15.7/ 13	8.5/ 7	8.2/ 7	25.7/ 22	22.2/ 19
−0.55	8.5/ 7	15.7/ 13	13.3/ 11	19.3/ 16	14.5/ 12	2.4/ 2	4.7/ 4	2.3/ 2	10.5/ 9
−0.45	4.9/ 4	23.0/ 19	3.6/ 3	6.0/ 5	6.0/ 5	0 / 0	2.4/ 2	3.5/ 3	2.3/ 2
−0.35	3.7/ 3	13.4/ 11	6.0/ 5	7.2/ 6	0 / 0	0 / 0	2.4/ 2	2.4/ 2	4.7/ 4
−0.25	2.5/ 2	6.1/ 5	7.3/ 6	3.6/ 3	1.2/ 1	1.2/ 1	2.4/ 2	4.8/ 4	0 / 0
−0.15	2.5/ 2	17.2/ 14	2.4/ 2	4.9/ 4	0 / 0	0 / 0	6.0/ 5	1.2/ 1	8.3/ 7
−0.05	10.0/ 8	19.8/ 16	4.9/ 4	17.2/ 14	7.3/ 6	8.5/ 7	3.6/ 3	7.2/ 6	15.5/ 13
+0.05	5.1/ 4	17.5/ 14	14.9/ 12	28.4/ 23	3.7/ 3	0 / 0	7.3/ 6	15.7/ 13	13.2/ 11
+0.15	12.8/ 10	29.1/ 23	22.6/ 18	42.4/ 34	19.9/ 16	13.6/ 11	7.4/ 6	14.6/ 12	23.1/ 19
+0.25	14.3/ 11	34.7/ 27	35.5/ 28	54.4/ 43	20.1/ 16	5.0/ 4	8.7/ 7	28.4/ 23	20.9/ 17
+0.35	14.5/ 11	54.9/ 42	54.2/ 42	66.8/ 52	37.0/ 29	8.9/ 7	13.8/ 11	30.0/ 24	18.6/ 15
+0.45	22.9/ 17	79.8/ 60	46.2/ 35	96.7/ 74	20.7/ 16	6.5/ 5	15.4/ 12	30.5/ 24	17.6/ 14
+0.55	23.6/ 17	80.5/ 59	72.9/ 54	69.7/ 52	34.6/ 26	7.9/ 6	9.2/ 7	24.7/ 19	19.3/ 15
+0.65	17.3/ 12	99.3/ 70	68.6/ 49	98.2/ 71	24.7/ 18	20.4/ 15	14.8/ 11	40.0/ 30	21.2/ 16
+0.75	25.9/ 17	62.8/ 42	50.0/ 34	82.9/ 57	36.2/ 25	22.8/ 16	32.5/ 23	64.2/ 46	52.7/ 38
+0.85	21.8/ 13	70.0/ 43	44.5/ 28	98.2/ 62	43.9/ 28	24.9/ 16	28.9/ 19	86.7/ 57	61.5/ 41
+0.95	7.9/ 4	47.9/ 24	23.2/ 11	53.2/ 27	56.6/ 29	42.8/ 22	58.5/ 30	160.6/ 86	204.8/111
Total	243.6/180	805.7/593	587.4/439	922.2/686	432.0/317	201.4/142	266.8/192	655.6/471	627.3/446

Center	1.937 GeV	1.952 GeV	1.970 GeV	2.001 GeV	2.022 GeV	2.051 GeV	2.084 GeV	2.106 GeV
	Number weighted/Number unweighted							
−0.95	46.3/ 40	21.0/ 18	17.3/ 15	11.6/ 10	8.2/ 7	12.6/ 11	7.4/ 6	7.7/ 6
−0.85	33.6/ 29	10.4/ 9	9.2/ 8	19.6/ 17	8.2/ 7	5.7/ 5	2.3/ 2	8.0/ 7
−0.75	29.0/ 25	12.7/ 11	19.8/ 17	16.1/ 14	8.0/ 7	4.6/ 4	4.6/ 4	11.6/ 10
−0.65	18.6/ 16	4.7/ 4	8.1/ 7	18.5/ 16	11.6/ 10	7.0/ 6	3.5/ 3	5.8/ 5
−0.55	8.2/ 7	2.3/ 2	3.5/ 3	7.0/ 6	5.8/ 5	4.6/ 4	3.9/ 3	4.6/ 4
−0.45	7.0/ 6	3.5/ 3	3.5/ 3	5.8/ 5	8.2/ 7	2.3/ 2	4.9/ 4	9.3/ 8
−0.35	4.7/ 4	2.4/ 2	2.4/ 2	7.0/ 6	7.0/ 6	5.8/ 5	5.9/ 5	5.8/ 5
−0.25	2.4/ 2	8.2/ 7	8.3/ 7	9.5/ 8	8.2/ 7	4.9/ 4	5.8/ 5	2.3/ 2
−0.15	8.3/ 7	7.1/ 6	5.9/ 5	16.4/ 14	7.0/ 6	3.8/ 3	5.8/ 5	5.8/ 5
−0.05	20.2/ 17	6.0/ 5	2.4/ 2	16.5/ 14	8.3/ 7	10.7/ 9	2.3/ 2	5.8/ 5
+0.05	15.6/ 13	13.1/ 11	14.4/ 12	26.1/ 22	14.2/ 12	11.8/ 10	4.8/ 4	11.7/ 10
+0.15	23.0/ 19	10.8/ 9	16.8/ 14	32.3/ 27	10.7/ 9	3.6/ 3	17.7/ 15	26.2/ 22
+0.25	23.2/ 19	12.4/ 10	15.7/ 13	22.9/ 19	21.6/ 18	18.1/ 15	12.0/ 10	17.8/ 15
+0.35	18.5/ 15	13.6/ 11	12.3/ 10	15.8/ 13	9.7/ 8	13.3/ 11	13.4/ 11	16.8/ 14
+0.45	15.0/ 12	6.2/ 5	8.7/ 7	12.5/ 10	6.1/ 5	7.4/ 6	12.2/ 10	3.6/ 3
+0.55	12.8/ 10	1.3/ 1	2.6/ 2	1.3/ 1	6.3/ 5	2.5/ 2	9.9/ 8	9.9/ 8
+0.65	7.9/ 6	5.3/ 4	3.9/ 3	1.3/ 1	1.3/ 1	2.6/ 2	2.6/ 2	8.9/ 7
+0.75	37.0/ 27	16.4/ 12	10.9/ 8	14.9/ 11	12.2/ 9	18.7/ 14	9.3/ 7	7.9/ 6
+0.85	63.8/ 43	31.3/ 21	29.5/ 20	62.4/ 43	40.4/ 28	38.9/ 27	35.2/ 25	42.4/ 30
+0.95	107.2/ 60	80.6/ 45	74.2/ 43	141.3/ 81	102.4/ 58	101.3/ 58	107.2/ 63	125.0/ 75
Total	502.2/377	269.2/196	269.2/201	458.8/338	305.3/222	280.2/201	270.8/194	336.9/247

TABLE V. $K^-p \to \pi^-\Sigma^+$ data binned in production cosine.

Center	Sum of polar cosine/Number unweighted 1.732 GeV	1.754 GeV	1.782 GeV	1.798 GeV	1.818 GeV	1.844 GeV	1.865 GeV	1.887 GeV	1.919 GeV
−0.95	1.5/ 6	−3.3/ 15	−1.8/ 8	−3.0/ 11	−1.8/ 9	0.6/ 7	−1.2/ 9	0.0/ 24	1.4/ 31
−0.85	−1.5/ 11	−2.2/ 17	−4.8/ 14	−7.9/ 29	−8.2/ 13	2.4/ 8	−0.2/ 10	−1.4/ 26	−0.5/ 13
−0.75	0.0/ 9	−0.2/ 16	−4.2/ 15	−5.5/ 18	−1.9/ 8	1.7/ 5	−0.5/ 8	3.7/ 21	0.8/ 16
−0.65	−1.1/ 5	−2.5/ 19	−4.2/ 10	−3.2/ 18	−1.9/ 6	1.2/ 4	−0.4/ 3	−3.6/ 9	0.4/ 7
−0.55	1.2/ 4	−4.6/ 16	−3.5/ 10	−2.4/ 6	−1.5/ 2	1.6/ 3	0.4/ 2	1.5/ 8	−1.2/ 5
−0.45	0.3/ 4	0.9/ 4	−2.4/ 5	−0.6/ 5	1.3/ 2	−0.8/ 1	−0.9/ 2	−2.2/ 6	0.5/ 2
−0.35	−0.9/ 7	−1.6/ 5	−0.8/ 7	−1.0/ 4	−0.3/ 1	0 / 0	−0.3/ 1	−0.9/ 2	−0.4/ 1
−0.25	1.0/ 1	−2.5/ 3	0.7/ 1	0.4/ 1	0 / 0	0 / 0	0 / 0	−0.8/ 1	−0.3/ 3
−0.15	−0.1/ 5	0.2/ 6	1.9/ 4	0.2/ 3	0 / 0	−0.7/ 1	−2.0/ 3	−0.1/ 3	−0.8/ 4
−0.05	−0.3/ 2	−1.1/ 5	1.4/ 4	2.3/ 7	−1.0/ 1	−0.3/ 4	−0.5/ 5	0.6/ 5	−3.6/ 10
+0.05	0.6/ 4	1.9/ 6	7.6/ 13	5.1/ 11	1.4/ 3	−0.1/ 2	−1.0/ 2	−2.6/ 5	−2.5/ 17
+0.15	1.7/ 4	6.4/ 16	3.2/ 6	1.4/ 18	−2.2/ 5	−2.0/ 7	−1.1/ 4	−2.0/ 12	−3.4/ 9
+0.25	1.8/ 5	5.3/ 22	8.6/ 29	5.1/ 24	0.1/ 12	−1.1/ 3	−1.8/ 5	−2.4/ 16	−3.4/ 18
+0.35	3.4/ 11	11.1/ 32	7.3/ 29	3.8/ 37	5.6/ 15	0.2/ 5	−1.2/ 5	−4.6/ 20	−4.0/ 17
+0.45	3.2/ 15	9.7/ 45	4.5/ 37	3.6/ 41	1.6/ 21	−0.2/ 6	−0.3/ 10	−2.8/ 28	−3.0/ 17
+0.55	2.6/ 19	22.0/ 56	7.8/ 36	14.4/ 59	0.9/ 32	−0.2/ 4	1.8/ 8	−0.7/ 17	−4.2/ 8
+0.65	5.0/ 17	8.5/ 48	19.5/ 42	10.4/ 55	8.7/ 25	4.0/ 10	6.3/ 13	7.7/ 20	4.0/ 15
+0.75	5.8/ 16	15.6/ 59	10.9/ 37	26.5/ 64	12.9/ 31	0.9/ 8	6.4/ 16	10.2/ 34	6.8/ 23
+0.85	5.1/ 11	9.9/ 37	6.7/ 26	12.0/ 40	10.4/ 30	2.0/ 11	11.0/ 30	15.1/ 60	3.6/ 37
+0.95	2.3/ 7	4.5/ 18	1.1/ 12	6.9/ 30	8.2/ 20	1.0/ 18	6.3/ 36	7.0/ 70	14.2/ 71
Total	0 /163	0 /445	0 /345	0 /481	0 /236	0 /107	0 /172	0 /387	0 /324

Center	Sum of polar cosine/Number unweighted 1.937 GeV	1.952 GeV	1.970 GeV	2.001 GeV	2.022 GeV	2.051 GeV	2.084 GeV	2.106 GeV
−0.95	−2.1/ 29	−2.3/ 11	−1.1/ 6	−4.0/ 9	0 / 2	0.5/ 8	−0.5/ 3	−1.4/ 2
−0.85	2.6/ 21	0.7/ 12	0.1/ 3	−1.3/ 10	−1.5/ 3	1.3/ 3	1.0/ 1	0.6/ 3
−0.75	−0.2/ 18	−1.9/ 4	−2.4/ 7	−1.4/ 8	−2.0/ 6	0.7/ 3	0 / 3	−0.8/ 3
−0.65	−4.1/ 11	−0.6/ 4	−0.6/ 2	−0.8/ 8	−1.4/ 5	0.7/ 5	0.8/ 4	0.8/ 2
−0.55	−1.8/ 5	−2.2/ 3	−0.6/ 1	−0.7/ 8	−0.7/ 6	−3.1/ 10	−0.4/ 3	−0.7/ 4
−0.45	−2.0/ 4	0 / 0	0.5/ 1	1.5/ 10	−1.9/ 7	−0.5/ 4	0.1/ 2	0.1/ 2
−0.35	−0.4/ 1	0 / 0	0 / 0	2.2/ 7	1.3/ 3	0.5/ 1	0 / 0	−0.3/ 1
−0.25	0 / 0	1.5/ 2	0.7/ 1	3.2/ 8	0.5/ 2	0.3/ 1	0.9/ 5	1.2/ 2
−0.15	−0.2/ 10	0.4/ 2	0.5/ 3	0.9/ 10	1.3/ 5	−0 / 3	1.1/ 3	2.0/ 4
−0.05	0.8/ 8	0.6/ 3	−2.1/ 5	3.0/ 13	−0.5/ 10	0.4/ 3	−1.3/ 4	0.2/ 3
+0.05	−0.1/ 11	−1.1/ 3	1.3/ 5	0.6/ 13	−0.7/ 11	−0.5/ 10	−0.6/ 2	−1.3/ 6
+0.15	−9.7/ 14	−3.1/ 7	−0.6/ 9	−0.4/ 10	−3.4/ 8	1.6/ 9	−1.5/ 8	−2.7/ 11
+0.25	−1.8/ 10	−0.2/ 7	−1.5/ 8	−0.7/ 18	−6.4/ 14	−0.8/ 7	−1.3/ 8	−0.3/ 7
+0.35	−4.8/ 11	−1.9/ 3	−3.6/ 11	−1.6/ 15	1.4/ 11	−3.9/ 8	−0.7/ 5	0.1/ 8
+0.45	−5.5/ 13	−0.7/ 2	−2.5/ 5	−1.2/ 7	0.9/ 3	−0.3/ 1	−2.1/ 3	−2.8/ 7
+0.55	−2.1/ 12	0.1/ 1	0 / 0	0.3/ 1	0 / 0	0.7/ 1	0.5/ 6	1.6/ 2
+0.65	2.7/ 9	1.8/ 4	0.7/ 1	0.9/ 3	0.6/ 1	−1.5/ 4	0.5/ 1	1.2/ 6
+0.75	5.9/ 13	3.2/ 6	1.3/ 4	−0.1/ 16	−0.3/ 9	−0.2/ 10	−0.7/ 6	2.3/ 11
+0.85	11.2/ 48	1.1/ 27	0.9/ 6	−7.9/ 33	−2.2/ 31	−3.1/ 25	−2.2/ 15	−6.2/ 21
+0.95	6.9/ 91	8.2/ 45	7.7/ 25	−2.8/ 82	−2.1/ 43	−9.2/ 58	−0.8/ 46	−5.0/ 45
Total	0 /339	0 /146	0 /103	0 /289	0 /180	0 /174	0 /128	0 /150

is not changed under the transformation from the over-all center-of-mass frame to the decay center-of-mass frame. We present in Table V the sum of $\cos\chi$ and the number of events in each of 20 bins of $\cos\theta$. For use in analysis we have grouped bins and determined the polarization and its uncertainty by[9]

$$P = \frac{3\sum_i \cos\chi_i}{\alpha N},$$

$$\Delta P = \left(\frac{3-Q}{\alpha^2 N}\right)^{1/2},$$

where the sum is over the N events in the grouped bins. The quantity Q is either $(\alpha P)^2$ or 1.0, whichever is smaller.

D. Legendre Coefficients

We have expanded each production angular distribution, properly normalized to the cross section, in the Legendre series

$$\frac{d\sigma}{d\Omega} = \lambda\!\!\!^{-2}\sum_n A_n P_n(\cos\theta), \tag{1a}$$

where $2\pi\lambda\!\!\!^{-}$ is the c.m. wavelength of the K^-. For the $\pi^-\Sigma^+$ final state we also expanded the product of this distribution with the polarizations, in the first associated Legendre series.

$$\vec{P}\frac{d\sigma}{d\Omega} = \lambda\!\!\!^{-2}\hat{n}\sum_n B_n P_n^1(\cos\theta). \tag{1b}$$

For this expansion $d\sigma/d\Omega$ was taken from the $\Sigma^+ \to \pi^+ n$ events and $\vec{P}$ from the $\Sigma^+ \to \pi^0 p$ events; also, because of limited statistics for the latter decay, information from adjacent groups of bins was not kept strictly independent.[2] The coefficients of these expansions are tabulated in Table VI and plotted in Fig. 3, along with the data from other experiments.[4,7,10] Expansion to higher than seventh order in no case significantly improved the fit or significantly changed any of the lower-order coefficients.

The partial-wave analysis of the data may be based either on cross sections, angular distributions, and polarizations or on the Legendre coefficients. We would expect the slight correlation of data, in the expansion of $\vec{P}\,d\sigma/d\Omega$, to render less meaningful the statistical indicators from the analysis of the coefficients. Also, although the distributions were normalized to the cross section, the greater uncertainty of the latter (fewer events due to tighter cuts, uncertainty in normalization, etc.) was not originally incorporated into the error structure of the coefficients. Incorporating this significantly increases the errors for some of the A_0's (note that Table VI presents the correct values; Fig. 3 shows the values used in our fitting). Clearly this counters the effects of the above-mentioned correction, increasing fit χ^2's because of too-small errors. Our original intent was to fit the Legendre coefficients only to obtain starting values for fitting in the cross sections, angular distributions, and polarizations directly. We discuss this further below.

IV. PARTIAL-WAVE ANALYSIS

A. Theory

The theory of partial-wave analysis for reactions of the form spin 0 + spin $\frac{1}{2} \to$ spin 0 + spin $\frac{1}{2}$ has been described in detail elsewhere.[11,12] We wish here to establish our conventions. The transition operator must take the form

$$T = f(E,\cos\theta) + g(E,\cos\theta)\vec{\sigma}\cdot\hat{n},$$

where $\vec{\sigma}$ is the Pauli spin matrix; $\cos\theta$ and $\hat{n}$ are defined as in Secs. III B and III C. The functions f and g, the spin-nonflip and spin-flip amplitudes, respectively, may depend on the c.m. energy E and the production angle. Because of rotational invariance the angular dependence takes the form

$$f(E,\cos\theta) = \frac{1}{(kk_\pi)^{1/2}}\sum_L [(L+1)T_L^+ + LT_L^-]P_L(\cos\theta),$$

$$g(E,\cos\theta) = \frac{i}{(kk_\pi)^{1/2}}\sum_L [T_L^+ - T_L^-]P_L^1(\cos\theta),$$

where k and k_π are magnitudes of the c.m. momenta for the K^- and π, respectively. The partial waves $T_L^\pm$ for our reactions are related to the isospin eigenwaves by

$$T_L^\pm(K^-p \to \pi^+\Sigma^-) = (\tfrac{1}{6})^{1/2}T_L^\pm(I=0) - \tfrac{1}{2}T_L^\pm(I=1),$$

$$T_L^\pm(K^-p \to \pi^-\Sigma^+) = (\tfrac{1}{6})^{1/2}T_L^\pm(I=0) + \tfrac{1}{2}T_L^\pm(I=1).$$

The states affected by $T_L^\pm$ have spin $J = L \pm \frac{1}{2}$ and parity $P = -(-1)^L$. The observables are expressed in terms of f and g as follows:

$$\frac{d\sigma}{d\Omega} = \frac{k_\pi}{k}(|f|^2 + |g|^2), \tag{2a}$$

$$P\frac{d\sigma}{d\Omega} = \frac{2k_\pi}{k}\,\mathrm{Re}(f^*g)\hat{n}. \tag{2b}$$

We may compare Eq. (2) with Eq. (1). Since the explicit dependence on k_π is canceled and $\lambda\!\!\!^{-}$ is inversely proportional to k, the A_n and B_n coefficients have a constant bilinear dependence on the $T_L^\pm$. This dependence has been tabulated, for example, in Ref. 11.

Certain general properties are assumed to hold for the transition operator. The conservation of probability requires $|T_L^\pm| \leq 0.5$ for inelastic transitions. The Wigner condition for causality restricts the variation of the phase, δ, of a partial wave[11]

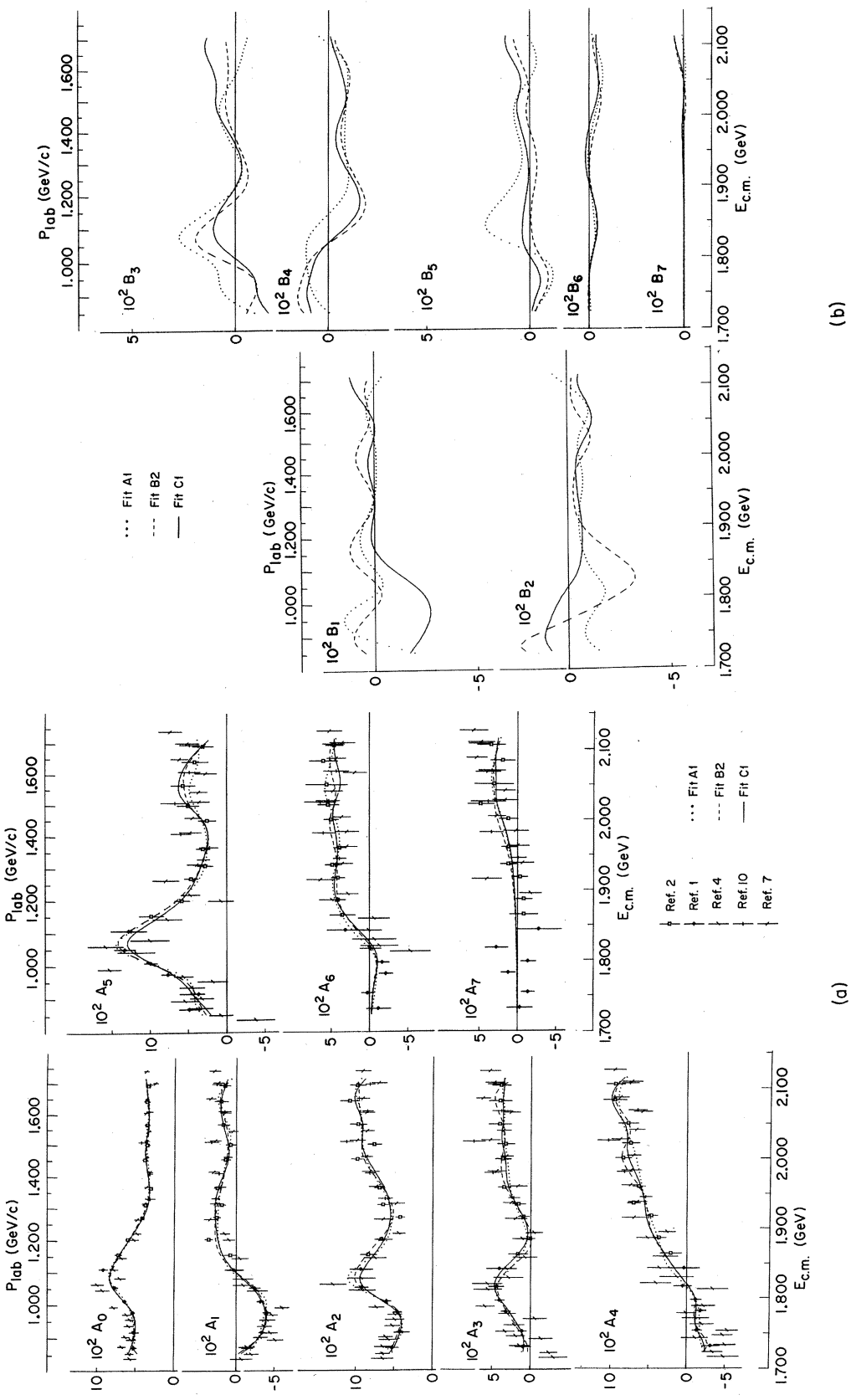

FIG. 3 *(continued)*

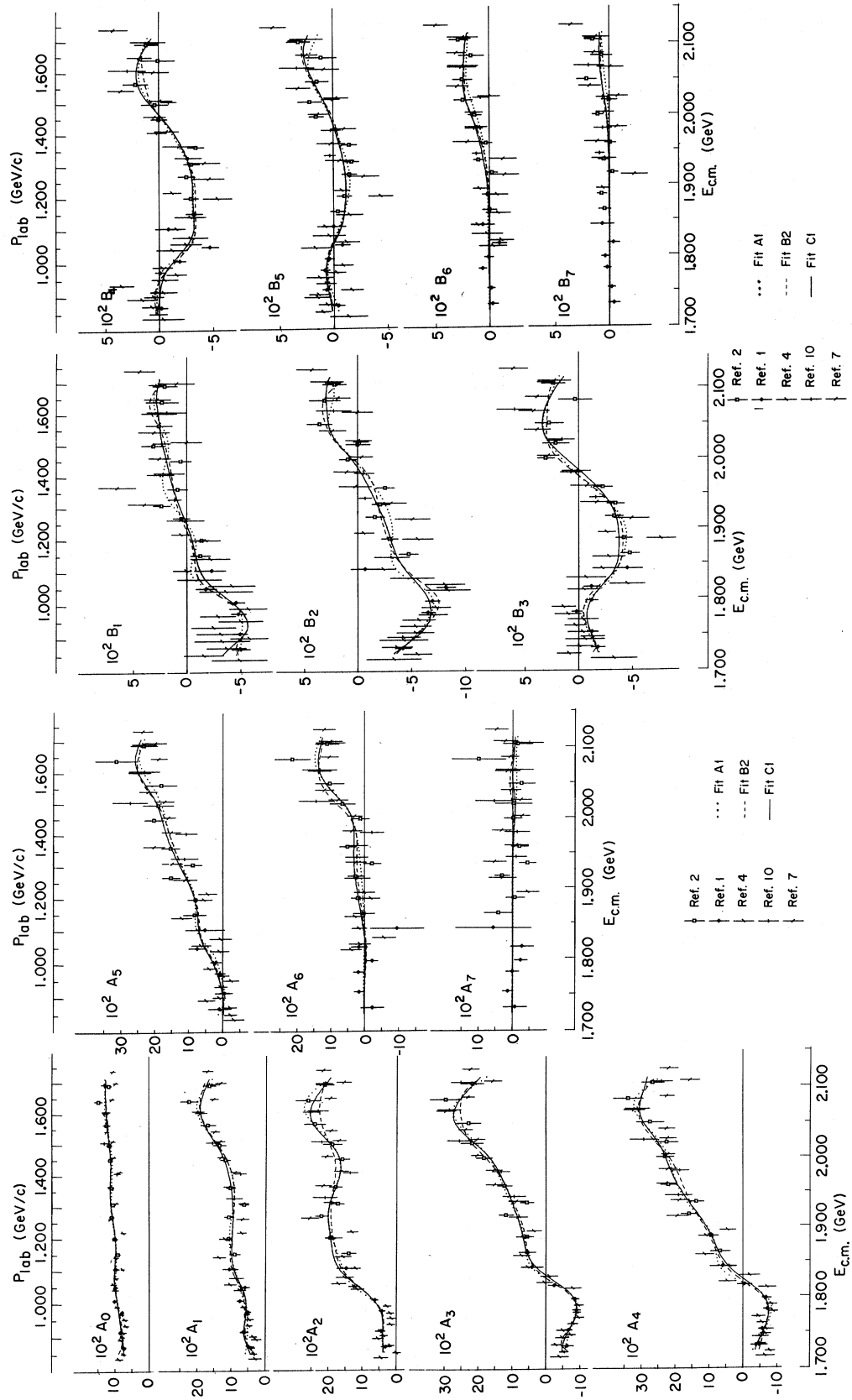

FIG. 3. (a) $K^-p \to \pi^+\Sigma^-$ Legendre series coefficients predicted by the three fits with highest probability from Table VII. All available data are superimposed. (b) $K^-p \to \pi^-\Sigma^+$ associated Legendre series coefficients predicted by the three fits with highest probability from Table VII. No data are available here since the Σ^+ polarization is not observed. (c) $K^-p \to \pi^-\Sigma^+$ Legendre series coefficients predicted by the three fits with highest probability from Table VII. All available data are superimposed. (d) $K^-p \to \pi^-\Sigma^+$ associated Legendre series coefficients predicted by the three fits with highest probability from Table VII. All available data are superimposed.

TABLE VI. Legendre coefficients.

A. From $K^-p \to \pi^+\Sigma^-$ angular distributions

$E_{c.m.}$ (GeV)	$10^{+3}A_0$	$10^{+3}A_1$	$10^{+3}A_2$	$10^{+3}A_3$	$10^{+3}A_4$	$10^{+3}A_5$	$10^{+3}A_6$	$10^{+3}A_7$
1.732	53± 6	−15± 7	54±10	10±10	−32±12	49±15	−12±16	−3±17
1.754	52± 6	−34± 5	42± 6	11± 6	−13± 7	37± 8	3± 8	−14± 8
1.782	54± 6	−41± 6	46± 7	33± 7	−18± 7	78±12	−22± 9	12± 9
1.798	65± 7	−33± 5	61± 8	41± 7	−12± 7	101±13	−17± 9	−14±10
1.818	78± 8	−25± 7	94±12	45±11	5±11	135±19	−1±13	28±15
1.844	94±12	3±12	95±18	41±18	4±20	130±28	32±24	−28±29
1.865	75± 6	8± 8	86±12	17±13	22±14	101±17	37±17	−8±18
1.887	61± 4	36± 5	67± 7	3± 8	37± 9	59±10	42±10	−8±10
1.919	42± 3	26± 4	44± 6	10± 7	48± 8	48± 9	42± 9	−3±10
1.937	38± 3	19± 5	65± 8	16± 8	71± 9	28±10	49±10	12±10
1.961	31± 3	24± 5	70± 7	35± 8	64± 9	31± 9	39± 8	12± 9
2.001	38± 3	14± 6	98±10	36±10	84±11	25±11	50±10	12±12
2.022	35± 4	7± 6	76±10	33±11	74±12	50±14	54±14	48±17
2.051	35± 4	16± 8	97±13	40±15	77±14	56±16	56±27	30±25
2.084	37± 4	20± 9	113±15	42±15	99±16	43±17	62±19	20±16
2.106	34± 4	15± 7	98±12	39±12	94±13	31±13	46±12	34±18

B. From $K^-p \to \pi^-\Sigma^+$ angular distributions

$E_{c.m.}$ (GeV)	$10^{+3}A_0$	$10^{+3}A_1$	$10^{+3}A_2$	$10^{+3}A_3$	$10^{+3}A_4$	$10^{+3}A_5$	$10^{+3}A_6$	$10^{+3}A_7$
1.732	75±10	41±11	32±13	−64±19	−48±24	10±32	−23±34	−8±34
1.754	87±10	65± 9	46± 9	−68±13	−59±14	−6±14	16±15	14±15
1.782	80± 9	51± 9	42± 9	−91±15	−73±15	8±15	18±15	−0±19
1.798	102±11	75±11	63±11	−87±14	−70±15	20±16	−24±16	−25±19
1.818	101±12	61±13	128±20	−24±19	−4±21	77±26	17±23	−28±33
1.844	97±15	107±24	151±33	42±32	61±38	54±56	−97±79	58±10
1.865	94±10	94±16	146±23	58±24	70±28	85±33	3±31	44±41
1.887	103± 7	112±12	200±18	57±18	96±20	82±23	21±19	−7±27
1.919	112± 8	112±13	230±21	123±21	166±23	158±26	29±23	33±22
1.937	105± 8	64±13	174±19	57±20	138±22	88±26	−22±25	−44±24
1.961	112± 8	108±14	188±20	127±22	228±25	159±27	53±24	−21±25
2.001	114± 9	120±15	162±22	184±24	231±27	203±29	13±26	−2±26
2.022	117±11	139±20	193±28	222±34	228±35	192±45	67±37	−2±54
2.051	126±13	175±24	248±34	234±38	280±43	185±46	105±41	−26±38
2.084	146±15	225±28	260±38	293±47	336±48	310±63	211±53	99±78
2.106	121±11	173±20	220±29	224±34	275±36	239±41	114±34	−15±42

C. From $K^-p \to \pi^-\Sigma^+$ (polarization) × (angular distribution)

$E_{c.m.}$ (GeV)	$10^{+3}B_0$	$10^{+3}B_1$	$10^{+3}B_2$	$10^{+3}B_3$	$10^{+3}B_4$	$10^{+3}B_5$	$10^{+3}B_6$	$10^{+3}B_7$
1.732	0± 0	−50±11	−42± 9	−18± 7	−2± 5	−4± 5	−3± 5	−4± 5
1.754	0± 0	−50± 9	−58± 9	−13± 5	4± 4	7± 4	−1± 3	−2± 3
1.782	0± 0	−48± 9	−66±10	2± 5	−1± 5	8± 4	6± 4	2± 3
1.798	0± 0	−46± 9	−69±10	−12± 6	−19± 6	4± 4	1± 4	4± 4
1.818	0± 0	−18±10	−82±13	−12± 8	−47± 9	−8± 7	−9± 7	−4± 6
1.844	0± 0	−23±13	−7±13	−45±15	−9±12	−0±11	6±11	7±11
1.865	0± 0	−13± 9	−47±10	−47±10	−32± 8	−4± 7	−0± 6	4± 6
1.887	0± 0	−14± 7	−30± 8	−42± 8	−29± 7	−10± 7	1± 6	7± 5
1.919	0± 0	5± 8	−16± 9	−33± 9	−25± 8	−15± 7	−3± 5	−3± 5
1.937	0± 0	23± 8	−21± 8	−34± 8	−30± 8	−17± 6	10± 5	5± 5
1.961	0± 0	8± 9	−26± 8	−22± 9	−34± 8	−15± 7	3± 6	−1± 5
2.001	0± 0	6± 9	9± 8	30± 8	−0± 7	15± 7	13± 6	11± 5
2.022	0± 0	31±11	−0±11	21±12	4±12	21±11	24± 9	0± 7
2.051	0± 0	25±12	35±12	27±13	21±12	15±10	25± 9	21± 9
2.084	0± 0	23±15	30±15	3±15	1±15	11±14	16±12	7±10
2.106	0± 0	20±11	21±11	23±11	11±11	32±11	28± 9	15± 8

$$\frac{\partial\delta}{\partial k} \geq -R\,,$$

where the range R may be the inverse mass of a field quantum. We emphasize that we have not imposed such conditions during the fitting process.

B. Procedure

The partial-wave analysis was done on a CDC 6600; the fitting program used a modified version of the code VARMIT, which minimized a function using a variable metric in the parameter space.[13] The function minimized was the χ^2:

$$\chi^2 = \sum_i [(c_i - x_i)/\Delta x_i]^2\,.$$

The sum is over all data points; x_i and Δx_i are the experimental value and its error; and c_i is the corresponding value calculated from the partial waves. The program could fit either the Legendre coefficients or the cross sections, angular distributions, and polarizations.

In our energy-dependent fits we have used a variety of parametrizations for the partial waves.

$$P\colon\ (q_1 + q_2 k + q_3 k^2)\exp[\,i(q_4 + q_5 k + q_6 k^2)]\,,$$

$$V\colon\ q_1(k - q_2)^2\exp[\,i(q_3 + q_4 k + q_5 k^2)]\,,$$

$$R\colon\ \frac{q_1 q_3 d_1(E) e^{iq_4}}{(q_2 - E) - iq_3 d_2(E)}\,.$$

The first two are background parametrizations and depend on the energy through the c.m. momentum of the K^-. The last is the Breit-Wigner resonant parametrization. In the fitting process the energy dependence of the coupling is not varied: The functions d_i are treated as constants for each energy. The resonant energy E_R is q_2 and we have fixed q_4 at either 0 or π. The (signed) amplitude at resonance is

$$t = q_1 \frac{d_1(q_2)}{d_2(q_2)}\, e^{iq_4}$$

and the full width evaluated at resonance is

$$\Gamma = 2q_3 d_2(q_2)\,.$$

In our fits we have assumed the partial-width energy dependence suggested by Glashow and Rosenfeld,[14]

$$\Gamma_i \propto \left(\frac{k_i^2}{k_i^2 + X^2}\right)^{l_i} \frac{k_i}{E}\,,$$

with $X = 0.35$ GeV/c; k_i is the c.m. momentum for the channel, with l_i its orbital angular momentum quantum number. For determining the full-width dependence, $d_2(E)$, rough approximations for decays into a variety of channels were used. Blatt and Weisskopf have derived the energy dependence of the partial width for the nonrelativistic case, which differs from the above for $l > 1$.[15] The values of t and Γ were not sensitive to our particular choice of energy dependence.[2]

Frequently both a resonant and a nonresonant parametrization were included in a partial wave, in which case they were simply added. Since the resonant parametrization contains an arbitrary phase, this need not violate unitarity (conservation of probability).[12] We have not needed to use this arbitrary phase, however.

In picking starting values for a fit, we have attempted to use information already available. First some of the partial waves have well-established resonances within our energy range.[16] These resonances are often seen in more than one reaction, which confirms their interpretation. We have consistently included the well-established resonances in $D_{05}, D_{15}, F_{05}, F_{17}, G_{07}$.[17] Other resonances were introduced as seemed appropriate. Second, because of the observed structure in the Legendre coefficients, it was clear that the higher-order waves emerge only at higher energies. For this we have used the V parametrization, starting its q_2 slightly below our energy range. All other parameters were started at zero.

The different fits are distinguished not so much by starting values as by starting structure. The structure of the better fits is given in Table VII; for each wave the letters indicate the type of parametrization, the numbers indicate how many parameters were free to vary. For $P(4)$ the quadratic coefficients were fixed to zero. The phases for all resonances were fixed to either 0 or π. Note that the fits $E1$ and $G1$ contain fixed resonances (0 free parameters) in D_{03} and D_{13}. These were the well-established resonances below our energy range.[16] In the B series the D_{03} resonance was included and varied, but the results were not very meaningful.

C. Results

The results of the partial-wave analysis for the three fits with highest probability are plotted in Fig. 4 and tabulated in Tables VIII–X. The Legendre coefficients predicted from these partial waves are plotted in Fig. 3, superimposed on all data presently available for the two reactions in the energy range covered by the analysis. Since the parameters obtained in the fits specify the energy dependence, both Fig. 4 and Tables VII–X present the partial waves at equally spaced energies. The statistical indicators are given in Table VII for the better fits to our Legendre coefficients. For these we have calculated the χ^2 for two additional sets of data: both for the original data – cross sections, angular distributions, and polarizations – and for all the Legendre coefficients

TABLE VII. Summary of partial-wave fits to Legendre coefficients.[a]

Fit	$A1$	$B1$	$B2$	$C1$	$C2$	$C4$	$E1$	$G1$
S_{01}	$P(6)$	$P(6)$	$P(6)$	$P(6)$	$P(6)$	$P(6)$	$P(6)$	$P(4)$
S_{11}	↓	↓	↓	↓	↓	↓	↓	↓
P_{01}								
P_{11}						$R(3)$		$R(3)+P(4)$
P_{03}						$P(6)$		$P(4)$
P_{13}						↓		$R(3)+V(5)$
D_{03}		$R(3)+P(6)$	$R(3)+P(6)$				$R(0)+V(5)$	$R(0)+V(5)$
D_{13}		$P(6)$	$P(6)$	$R(3)$	$R(3)$	$R(3)$	↓	$R(0)+R(3)$
D_{05}	$R(3)+P(6)$	$R(3)+V(5)$	$R(3)+V(5)$	$R(3)+V(5)$	$R(3)+V(5)$	$R(3)+V(5)$	$R(3)+V(5)$	$R(3)+V(5)$
D_{15}	↓	↓	↓	↓		↓	↓	↓
F_{05}			$R(3)+R(3)$	$R(3)+R(3)$		$R(3)+R(3)$		
F_{15}	$R(3)$	$V(5)$	↓	↓	↓	↓	$V(5)$	
F_{07}	$P(6)$	↓	$V(5)$	$V(5)$	$V(5)$	$V(5)$	↓	$R(3)$
F_{17}	$R(3)$	$R(3)$	$R(3)$	$R(3)$	$R(3)$	$R(3)$	$R(3)$	↓
G_{07}	↓	↓	↓	↓	↓	↓	↓	
G_{17}	...	...	...	...	...	...	$V(5)$	
NV	90	91	90	84	88	81	91	83
χ^2/DF	296/278	300/277	288/278	303/284	306/280	320/287	312/277	317/285
Prob.	21%	17%	33%	21%	14%	8%	7%	9%
$\langle\chi^2\rangle^1$	0.94	0.97	0.93	0.95	0.98	0.98	1.01	1.11
$\langle\chi^2\rangle^2$	1.57	1.58	1.56	1.54	1.54	1.56	1.81	1.62

[a] NV is the number of variables; DF is the number of degrees of freedom. $\langle\chi^2\rangle^1$ is the mean χ^2 contribution from cross sections, angular distributions, and polarizations. $\langle\chi^2\rangle^2$ is the mean χ^2 contribution from all Legendre coefficients in Fig. 3.

shown in Fig. 3. The average contributions are given in Table VII.

As pointed out in Sec. III D above, the statistical significance of the fits to the Legendre coefficients is somewhat questionable. However, continuing several of these fits by using the original data showed that the results from a fit to the coefficients were not misleading.[2] The partial waves were quite similar and the probabilities of fit were not drastically different (4% and 14% for the continuations of fits $A1$ and $C1$, respectively). We also continued two fits with all the coefficients shown in Fig. 3. Although the average χ^2 contribution remained relatively large (1.3 at best), the resulting partial waves were in good agreement with the fits to our own data.[2] Because of the large amounts of time required for the fits to the larger data samples, we have concentrated our efforts on fitting our Legendre coefficients.

We point out that the coefficients predicted by different fits are very similar where data are available; this may be seen in Fig. 3 for the three fits with highest probability. One can see that increased statistics, giving smaller errors, would not distinguish these solutions at most energies. Only in the B_n for the Σ^- final state where polarization data are unavailable do the solutions show marked differences. This means that a unique solution cannot be obtained without supporting data from other reactions. There is some information available in the literature for the reactions $K^-n \to \pi^0\Sigma^0$ in the lower half of our energy range.[18] We have calculated the χ^2 from these data within the range of our fits. The average contributions from the cross sections (22 data points) and from the angular distributions (151 data points) for our three solutions with highest probability were

Average contribution to χ^2.

	Cross sections	Angular distributions
$A1$	1.60	1.09
$B2$	2.10	0.88
$C1$	1.61	1.06

These data are not sufficient to distinguish among these three fits.

We also comment on the general properties of the partial waves. There is certainly no violation of unitarity: None of the waves approach the unitary limit. To look for violations of causality in Fig. 4, consider the Wigner limit to be one radian per pion mass clockwise. Since the symbols in Fig. 4 are spaced by 25 MeV, a clockwise movement of more than about 10 deg between symbols constitutes a local violation. Most waves actually move counterclockwise, especially for $J \geq \frac{5}{2}$. In several low-order waves, notably in D_{03}, these are

TABLE VIII. Partial waves calculated from fitted parameters for fit A1.

$E_{c.m.}$ (GeV)	S_{01}		P_{01}		P_{03}		D_{03}		D_{05}		F_{05}		F_{07}		G_{07}	
1.725	0.097	0.092	0.201	0.080	0.130	0.167	0.168	−0.077	0.012	−0.070	−0.068	−0.146	0.004	0.002	0.004	0.000
1.750	0.079	0.076	0.223	−0.054	0.138	0.118	0.139	−0.036	−0.003	−0.074	−0.144	−0.100	0.005	0.002	0.005	0.000
1.775	0.066	0.061	0.181	−0.151	0.136	0.081	0.105	−0.016	−0.021	−0.087	−0.165	−0.095	0.007	0.003	0.007	0.001
1.800	0.056	0.047	0.127	−0.200	0.129	0.053	0.073	−0.008	−0.030	−0.120	−0.126	−0.180	0.010	0.004	0.008	0.001
1.825	0.050	0.034	0.089	−0.214	0.122	0.034	0.044	−0.006	0.000	−0.166	0.034	−0.249	0.014	0.004	0.010	0.001
1.850	0.045	0.024	0.076	−0.209	0.116	0.020	0.018	−0.004	0.069	−0.165	0.140	−0.193	0.018	0.005	0.012	0.002
1.875	0.042	0.015	0.086	−0.188	0.113	0.011	−0.004	0.001	0.105	−0.117	0.154	−0.149	0.023	0.006	0.014	0.003
1.900	0.040	0.007	0.108	−0.153	0.113	0.005	−0.021	0.011	0.103	−0.076	0.147	−0.133	0.029	0.007	0.017	0.004
1.925	0.040	−0.001	0.129	−0.099	0.117	0.002	−0.031	0.026	0.088	−0.052	0.141	−0.128	0.035	0.007	0.020	0.006
1.950	0.041	−0.010	0.130	−0.034	0.124	0.000	−0.031	0.045	0.073	−0.043	0.141	−0.124	0.042	0.007	0.023	0.008
1.975	0.041	−0.022	0.099	0.025	0.135	0.001	−0.019	0.063	0.062	−0.044	0.148	−0.117	0.050	0.007	0.027	0.012
2.000	0.038	−0.036	0.043	0.049	0.150	0.004	0.004	0.075	0.061	−0.051	0.161	−0.103	0.058	0.007	0.031	0.018
2.025	0.031	−0.054	0.001	0.025	0.167	0.011	0.035	0.074	0.069	−0.056	0.174	−0.078	0.066	0.006	0.034	0.026
2.050	0.016	−0.072	0.013	−0.014	0.187	0.023	0.066	0.056	0.086	−0.054	0.182	−0.042	0.075	0.004	0.035	0.037
2.075	−0.010	−0.086	0.067	0.003	0.209	0.041	0.086	0.021	0.106	−0.039	0.177	0.002	0.084	0.002	0.031	0.051
2.100	−0.046	−0.091	0.065	0.099	0.231	0.066	0.086	−0.023	0.121	−0.009	0.152	0.046	0.094	−0.000	0.020	0.063

$E_{c.m.}$ (GeV)	S_{11}		P_{11}		P_{13}		D_{13}		D_{15}		F_{15}		F_{17}		G_{17}	
1.725	0.059	0.181	−0.059	−0.062	−0.004	−0.009	0.041	−0.013	0.007	0.012	−0.024	−0.004	−0.008	−0.000	0	0
1.750	0.096	0.166	−0.045	−0.076	0.021	0.020	0.030	−0.053	0.001	0.075	−0.031	−0.006	−0.009	−0.001	0	0
1.775	0.128	0.142	−0.035	−0.083	0.056	0.025	−0.005	−0.075	−0.006	0.105	−0.039	−0.010	−0.011	−0.001	0	0
1.800	0.153	0.111	−0.030	−0.084	0.088	0.010	−0.043	−0.074	−0.007	0.101	−0.049	−0.017	−0.014	−0.001	0	0
1.825	0.169	0.075	−0.031	−0.081	0.108	−0.016	−0.069	−0.062	0.001	0.080	−0.060	−0.029	−0.016	−0.002	0	0
1.850	0.175	0.038	−0.038	−0.073	0.117	−0.044	−0.084	−0.049	0.013	0.052	−0.070	−0.049	−0.020	−0.003	0	0
1.875	0.173	0.001	−0.046	−0.061	0.118	−0.068	−0.089	−0.043	0.025	0.025	−0.073	−0.080	−0.024	−0.005	0	0
1.900	0.162	−0.033	−0.053	−0.044	0.114	−0.086	−0.086	−0.046	0.035	0.001	−0.057	−0.117	−0.029	−0.007	0	0
1.925	0.143	−0.062	−0.056	−0.022	0.109	−0.097	−0.076	−0.055	0.045	−0.019	−0.017	−0.141	−0.036	−0.011	0	0
1.950	0.119	−0.084	−0.050	−0.001	0.103	−0.100	−0.057	−0.067	0.054	−0.035	0.026	−0.135	−0.044	−0.018	0	0
1.975	0.092	−0.098	−0.035	0.015	0.099	−0.097	−0.028	−0.073	0.064	−0.046	0.053	−0.114	−0.053	−0.031	0	0
2.000	0.063	−0.104	−0.016	0.020	0.094	−0.088	0.004	−0.068	0.074	−0.052	0.064	−0.092	−0.060	−0.052	0	0
2.025	0.036	−0.103	−0.002	0.012	0.089	−0.073	0.030	−0.046	0.085	−0.053	0.067	−0.074	−0.053	−0.086	0	0
2.050	0.012	−0.094	−0.001	−0.003	0.082	−0.055	0.037	−0.015	0.096	−0.049	0.067	−0.061	−0.018	−0.115	0	0
2.075	−0.006	−0.079	−0.017	−0.009	0.071	−0.036	0.021	0.006	0.107	−0.038	0.064	−0.051	0.028	−0.109	0	0
2.100	−0.018	−0.060	−0.036	0.007	0.053	−0.017	0.001	0.003	0.116	−0.023	0.062	−0.043	0.052	−0.082	0	0

TABLE IX. Partial waves calculated from fitted parameters for fit $B2$.

$E_{c.m.}$ (GeV)	S_{01}		P_{01}		P_{03}		D_{03}		D_{05}		F_{05}		F_{07}		G_{07}	
1.725	−0.001	0.002	0.252	−0.132	0.125	0.144	0.092	−0.101	−0.019	−0.030	−0.068	−0.033	−0.001	0.001	0.005	0.000
1.750	0.047	−0.020	0.245	−0.155	0.117	0.139	0.087	−0.008	−0.025	−0.035	−0.092	−0.069	−0.000	0.003	0.006	0.000
1.775	0.089	0.027	0.238	−0.167	0.111	0.135	0.053	−0.007	−0.036	−0.053	−0.103	−0.140	0.002	0.006	0.007	0.000
1.800	0.085	0.092	0.233	−0.168	0.107	0.132	0.039	−0.022	−0.030	−0.099	−0.050	−0.235	0.007	0.007	0.009	0.001
1.825	0.055	0.138	0.230	−0.160	0.105	0.130	0.032	−0.037	0.043	−0.133	0.075	−0.267	0.012	0.008	0.011	0.001
1.850	0.026	0.161	0.228	−0.144	0.105	0.130	0.025	−0.051	0.105	−0.085	0.172	−0.212	0.019	0.006	0.014	0.002
1.875	0.014	0.169	0.225	−0.120	0.106	0.131	0.014	−0.060	0.113	−0.034	0.210	−0.143	0.026	0.004	0.017	0.003
1.900	0.023	0.166	0.219	−0.090	0.109	0.133	−0.002	−0.064	0.106	−0.002	0.220	−0.088	0.033	0.000	0.021	0.004
1.925	0.050	0.151	0.209	−0.057	0.113	0.136	−0.023	−0.060	0.097	0.018	0.220	−0.046	0.040	−0.003	0.025	0.007
1.950	0.083	0.117	0.192	−0.023	0.118	0.139	−0.043	−0.044	0.090	0.033	0.216	−0.012	0.049	−0.005	0.031	0.010
1.975	0.104	0.063	0.167	0.008	0.125	0.144	−0.055	−0.016	0.085	0.044	0.210	0.018	0.057	−0.005	0.038	0.017
2.000	0.093	0.001	0.134	0.033	0.133	0.149	−0.053	0.017	0.082	0.052	0.201	0.045	0.067	−0.003	0.046	0.028
2.025	0.048	−0.034	0.095	0.046	0.143	0.155	−0.032	0.046	0.081	0.059	0.189	0.070	0.077	0.003	0.051	0.047
2.050	0.004	−0.018	0.056	0.045	0.154	0.161	0.002	0.059	0.082	0.065	0.173	0.092	0.086	0.015	0.044	0.076
2.075	0.017	0.023	0.021	0.028	0.167	0.167	0.036	0.048	0.085	0.069	0.154	0.110	0.093	0.032	0.014	0.099
2.100	0.080	0.001	−0.002	−0.004	0.182	0.173	0.052	0.019	0.091	0.071	0.134	0.124	0.095	0.056	−0.023	0.095

$E_{c.m.}$ (GeV)	S_{11}		P_{11}		P_{13}		D_{13}		D_{15}		F_{15}		F_{17}		G_{17}	
1.725	−0.039	0.164	0.091	−0.016	0.074	0.089	−0.137	−0.090	0.033	0.060	0.015	0.013	−0.005	−0.000	0	0
1.750	0.010	0.167	0.062	−0.049	0.098	0.063	−0.084	−0.085	−0.007	0.095	0.013	0.017	−0.006	−0.000	0	0
1.775	0.053	0.156	0.032	−0.062	0.110	0.038	−0.040	−0.071	−0.037	0.079	0.008	0.020	−0.008	−0.001	0	0
1.800	0.087	0.137	0.007	−0.061	0.115	0.018	−0.010	−0.047	−0.033	0.058	−0.002	0.019	−0.009	−0.001	0	0
1.825	0.112	0.114	−0.011	−0.054	0.115	0.004	0.003	−0.021	−0.019	0.044	−0.014	0.012	−0.012	−0.002	0	0
1.850	0.129	0.090	−0.023	−0.045	0.112	−0.005	−0.001	0.002	−0.005	0.033	−0.022	−0.009	−0.014	−0.002	0	0
1.875	0.139	0.065	−0.030	−0.038	0.109	−0.007	−0.017	0.011	0.007	0.022	−0.014	−0.040	−0.018	−0.004	0	0
1.900	0.144	0.043	−0.035	−0.032	0.106	−0.005	−0.034	0.004	0.017	0.011	0.022	−0.062	−0.023	−0.006	0	0
1.925	0.146	0.024	−0.039	−0.028	0.102	0.002	−0.040	−0.017	0.025	0.001	0.063	−0.052	−0.029	−0.011	0	0
1.950	0.144	0.008	−0.042	−0.026	0.097	0.012	−0.029	−0.040	0.033	−0.007	0.086	−0.024	−0.036	−0.021	0	0
1.975	0.140	−0.006	−0.046	−0.026	0.089	0.025	−0.002	−0.052	0.041	−0.014	0.092	0.003	−0.041	−0.041	0	0
2.000	0.136	−0.016	−0.051	−0.028	0.078	0.038	0.027	−0.043	0.049	−0.018	0.087	0.025	−0.027	−0.071	0	0
2.025	0.130	−0.023	−0.055	−0.033	0.063	0.050	0.043	−0.016	0.059	−0.019	0.080	0.040	0.013	−0.078	0	0
2.050	0.125	−0.028	−0.058	−0.042	0.045	0.059	0.036	0.012	0.070	−0.015	0.071	0.050	0.036	−0.055	0	0
2.075	0.120	−0.031	−0.060	−0.053	0.023	0.063	0.014	0.023	0.082	−0.005	0.062	0.057	0.039	−0.035	0	0
2.100	0.115	−0.032	−0.058	−0.069	0.002	0.060	−0.002	0.012	0.092	0.012	0.055	0.061	0.036	−0.024	0	0

TABLE X. Partial waves calculated from fitted parameters for fit *C*1.

$E_{c.m.}$ (GeV)	S_{01}		P_{01}		P_{03}		D_{03}		D_{05}		F_{05}		F_{07}		G_{07}	
1.725	0.156	−0.012	0.093	−0.070	0.147	0.119	0.158	−0.161	−0.037	−0.003	−0.087	−0.038	−0.000	0.000	0.005	0.000
1.750	0.140	0.028	0.099	−0.086	0.140	0.112	0.156	−0.096	−0.048	−0.011	−0.115	−0.076	−0.000	0.002	0.006	0.000
1.775	0.119	0.052	0.103	−0.098	0.136	0.106	0.134	−0.053	−0.059	−0.032	−0.132	−0.147	0.002	0.004	0.008	0.000
1.800	0.101	0.068	0.104	−0.107	0.133	0.102	0.105	−0.027	−0.054	−0.077	−0.096	−0.250	0.006	0.005	0.009	0.001
1.825	0.088	0.067	0.104	−0.111	0.132	0.099	0.075	−0.014	0.005	−0.115	0.024	−0.313	0.011	0.004	0.011	0.001
1.850	0.079	0.066	0.103	−0.112	0.132	0.097	0.046	−0.008	0.067	−0.088	0.145	−0.280	0.017	−0.000	0.014	0.002
1.875	0.074	0.062	0.101	−0.110	0.134	0.095	0.019	−0.004	0.086	−0.049	0.206	−0.208	0.022	−0.006	0.017	0.002
1.900	0.074	0.056	0.099	−0.104	0.138	0.095	−0.004	0.001	0.089	−0.023	0.227	−0.144	0.026	−0.012	0.020	0.004
1.925	0.076	0.047	0.095	−0.095	0.143	0.095	−0.024	0.011	0.088	−0.007	0.230	−0.094	0.031	−0.018	0.025	0.005
1.950	0.079	0.035	0.091	−0.083	0.149	0.096	−0.039	0.025	0.087	0.005	0.227	−0.055	0.036	−0.024	0.031	0.009
1.975	0.083	0.020	0.084	−0.070	0.156	0.097	−0.045	0.045	0.087	0.015	0.220	−0.022	0.043	−0.028	0.038	0.014
2.000	0.086	0.002	0.074	−0.055	0.165	0.099	−0.041	0.067	0.088	0.024	0.210	0.006	0.053	−0.030	0.046	0.023
2.025	0.085	−0.020	0.062	−0.040	0.176	0.101	−0.024	0.089	0.088	0.034	0.197	0.031	0.065	−0.026	0.055	0.038
2.050	0.077	−0.044	0.046	−0.025	0.187	0.103	0.005	0.103	0.087	0.044	0.182	0.053	0.078	−0.017	0.057	0.066
2.075	0.061	−0.069	0.026	−0.011	0.200	0.105	0.044	0.104	0.085	0.054	0.164	0.070	0.090	0.001	0.039	0.100
2.100	0.035	−0.090	0.003	−0.001	0.215	0.107	0.086	0.085	0.082	0.066	0.144	0.083	0.097	0.028	−0.006	0.115

$E_{c.m.}$ (GeV)	S_{11}		P_{11}		P_{13}		D_{13}		D_{15}		F_{15}		F_{17}		G_{17}	
1.725	0.215	0.168	−0.151	0.006	0.017	0.032	−0.016	−0.002	0.017	0.033	0.009	0.010	−0.004	−0.000	0	0
1.750	0.190	0.165	−0.091	−0.109	0.039	0.033	−0.019	−0.003	0.009	0.070	0.008	0.015	−0.005	−0.000	0	0
1.775	0.174	0.155	−0.000	−0.133	0.059	0.024	−0.023	−0.005	−0.016	0.066	0.003	0.021	−0.007	−0.001	0	0
1.800	0.164	0.141	0.058	−0.109	0.074	0.010	−0.027	−0.008	−0.009	0.045	−0.008	0.025	−0.008	−0.001	0	0
1.825	0.159	0.123	0.081	−0.079	0.083	−0.005	−0.032	−0.011	0.005	0.030	−0.025	0.023	−0.010	−0.001	0	0
1.850	0.156	0.102	0.083	−0.061	0.088	−0.017	−0.038	−0.017	0.017	0.017	−0.045	0.006	−0.012	−0.002	0	0
1.875	0.155	0.079	0.073	−0.057	0.091	−0.025	−0.045	−0.026	0.025	0.006	−0.053	−0.029	−0.015	−0.003	0	0
1.900	0.154	0.055	0.055	−0.062	0.094	−0.028	−0.050	−0.040	0.032	−0.005	−0.033	−0.068	−0.019	−0.004	0	0
1.925	0.151	0.028	0.028	−0.067	0.096	−0.027	−0.050	−0.060	0.037	−0.014	0.011	−0.087	−0.024	−0.008	0	0
1.950	0.145	0.001	−0.005	−0.061	0.098	−0.020	−0.038	−0.083	0.042	−0.020	0.055	−0.075	−0.030	−0.013	0	0
1.975	0.135	−0.027	−0.032	−0.040	0.098	−0.009	−0.011	−0.099	0.049	−0.025	0.080	−0.046	−0.037	−0.025	0	0
2.000	0.120	−0.054	−0.039	−0.006	0.095	0.006	0.019	−0.096	0.056	−0.027	0.087	−0.015	−0.039	−0.048	0	0
2.025	0.099	−0.078	−0.022	0.019	0.089	0.023	0.038	−0.081	0.065	−0.024	0.082	0.008	−0.015	−0.075	0	0
2.050	0.072	−0.098	0.002	0.017	0.076	0.040	0.047	−0.064	0.075	−0.017	0.073	0.025	0.023	−0.069	0	0
2.075	0.041	−0.111	0.006	0.002	0.057	0.055	0.049	−0.050	0.085	−0.004	0.063	0.035	0.037	−0.046	0	0
2.100	0.005	−0.116	−0.004	0.004	0.034	0.063	0.048	−0.040	0.092	0.016	0.053	0.041	0.037	−0.030	0	0

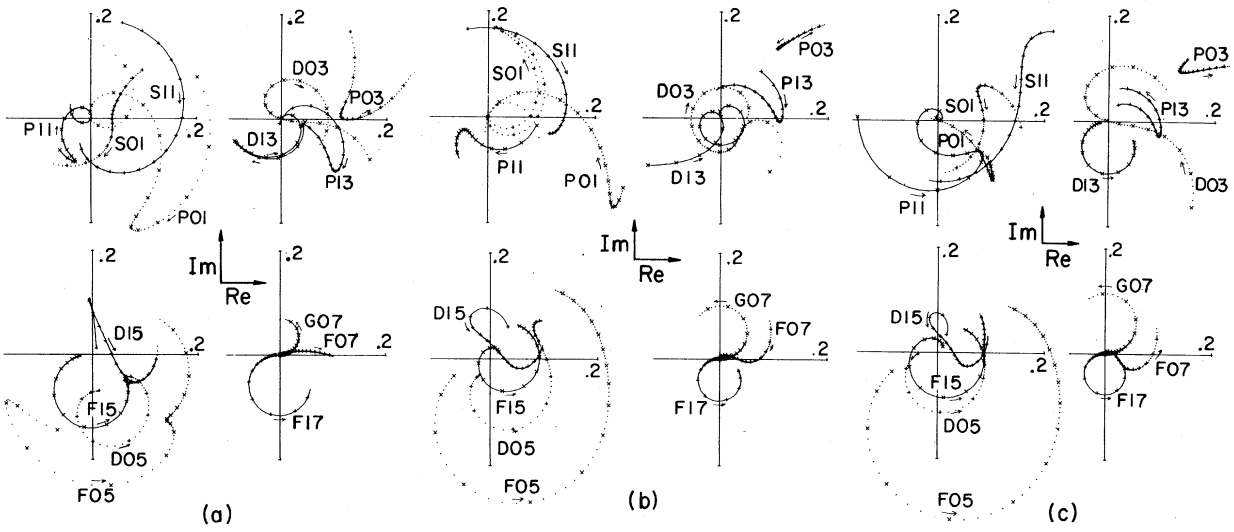

FIG. 4. Argand diagrams for selected partial-wave fits to $K^-p \to \pi^\pm\Sigma^\mp$ reactions. The labels for the fits correspond to those in Table VII; (a) fit $A1$, (b) fit $B2$, (c) fit $C1$. The symbols are plotted at energies starting from 1.725 GeV and separated by 0.025 GeV. Note that dotted curves are isospin-0 waves and solid curves are isospin-1 waves.

clockwise movements. However, since these occur close to the origin or near the end of our energy range, we do not consider them serious violations: Other energy variations not available to the parametrization are within errors of the waves shown. The violations in the fits shown in Fig. 4 are typical of those in all the fits listed in Table VII.[2]

Finally we have listed in Table XI the means of the quantities describing the resonances: E_R, t, and Γ. The errors indicate the spread of values for different fits and are not statistically significant. In particular, two of the resonances had reasonable parameters only in a single fit and so have no error. (For details see Ref. 2.) The first five resonances listed in the table are those that were previously well established. The values we have obtained for their resonant parameters are not notably different from values previously determined.[16] The last three resonances listed are near the extremes of our energy range and are not strongly supported by our data alone. The two resonant structures near the upper end of our range, in F_{15} and F_{05}, have been previously reported.[7] The resonance listed for P_{11}, at the lower end of our energy range, probably cannot be associated with the P_{11} resonance reported in the $\Lambda\pi$ final state.[19] In contrast with these last three resonances, the resonant structures seen in the F_{15} and D_{13} waves are well within our energy range and are strongly supported by our data. Both have been seen previously, the first references being Refs. 20 and 10, respectively. Other partial-wave analyses have been less able to see the structure in these two waves because the energy ranges studied ended or began in the region where the waves resonate, whereas our data are well concentrated in these regions. Although we obtain good solutions with background parametrizations in these waves, the "background" waves look very similar to the resonances: The wave moves counterclockwise through the imaginary axis at about the same energy. A resonance is more specifically characterized by the energy dependence of the phase: acceleration to resonance, then deceleration. However, the detailed nature of this variation is not well understood (see below) and, further, this variation may be affected by background (n.b., the presence of a distant resonance in the same wave). We feel that a fit with the more structural parametrization of a resonance is preferable to one with a general parametrization, even if the latter is slightly better statistically. The resonant struc-

TABLE XI. Resonance parameters.

Wave	E_R (GeV)	t	Γ (GeV)
D_{15}	1.765±0.009	0.074±0.017	0.120±0.038
D_{05}	1.832±0.005	−0.138±0.018	0.088±0.010
F_{05}	1.823±0.003	−0.268±0.027	0.104±0.016
F_{17}	2.034±0.014	−0.086±0.014	0.118±0.012
G_{07}	2.092±0.012	0.096±0.037	0.144±0.026
F_{15}	1.925±0.008	−0.137±0.015	0.146±0.022
D_{13}	1.985±0.005	−0.093±0.006	0.208±0.022
F_{05}	2.141±0.006	0.156±0.013	0.504±0.010
F_{15}	2.057	0.104	0.906
P_{11}	1.772	−0.108	0.080

tures in F_{15} and D_{13} are in this sense well supported by our analysis.

V. SU_3 SYMMETRIES

The first six resonances in Table XI have all been previously assigned to multiplets of particles based on the symmetry of the SU_3 group. We have tried to obtain SU_3-invariant coupling constants based on the results obtained from our fits and results from reactions involving the related resonances. The theoretical details on which this attempt is made have been described,[21] and similar attempts have been carried out by several groups.[22,23] All of the information we have used in our attempt is listed in Table XII. This includes the values from Table XI plus recent results on the decay of the $\Delta(F_7)$ into $\Sigma^+ K^+$.[24] All other values are taken from the compilation in Ref. 16. Where these authors have not given means and errors, we have estimated them from the spread of values found in different experiments.

If SU_3 were a perfect symmetry, first all the particles in a multiplet would have the same mass, and second, the couplings for various decay modes would be related by certain SU_3 projection coefficients.[21] We might assume that, although the masses vary within a multiplet, the breaking of SU_3 for the coupling constants might arise only through the different kinematics. In this case the reduced coupling constants should be related by the SU_3 projection coefficients. For a general reaction

$$t\Gamma = \pm (\Gamma_i \Gamma_j)^{1/2} = c_i c_j g^2 [V_i(E_R) V_j(E_R)]^{1/2},$$

where g^2 is the SU_3-invariant coupling constant and c_i, c_j are the projection coefficients. The kinematics factor we have used in fitting is

$$V_i(E) = \left(\frac{k_i^2}{k_i^2 + X^2}\right)^{l_i} \frac{k_i}{E} m_N,$$

which is the Glashow and Rosenfeld (GR) dependence mentioned above, using the nucleon mass m_N as a scale factor. Since we are studying the scattering of an octet $(K, \pi, \ldots)$ with an octet $(N, \Sigma, \ldots)$, this formulation is not satisfactory for couplings with resonant octets: Two couplings with octets are possible. In this case

$$t\Gamma = (c_i^f g_f + c_i^d g_d)(c_j^f g_f + c_j^d g_d)[V_i(E_R) V_j(E_R)]^{1/2},$$

where g_f and g_d are the antisymmetric and the symmetric couplings, respectively.[21] We have tried to obtain values of g_f and g_d for the D_5 and F_5 octets, and the values of g^2 for the F_7 decuplet and G_7 singlet. We have fit directly to the values of $t\Gamma$, which agrees with the procedure used in Ref. 23. This procedure eliminates the dependence, required for fitting the Γ_i, on sometimes poorly known elastic amplitudes. It has the added advantage of introducing explicitly the relative signs of couplings.

We have plotted in Fig. 5 the values of g_f, g_d, and g^2 obtained from the various values in Table XII, using the GR energy dependence with $X = 0.35$. For the resonant octets the results in general are parabolas in the (g_f, g_d) plane. We have assumed $g_d > 0$, which fixes the curves for inelastic reactions. The results from elastic reactions are straight lines, and we have chosen the intercept (sign of square root) that gives the best intersection with other curves. The best values of the coupling constants, using this energy dependence, are given in Table XIII. However, Fig. 5 shows that the assumption that the symmetry breaking arises only through the kinematics is not well supported.

The energy dependence of the partial widths, however, is not well established; we have also fit the values of Table XII using the GR energy dependence with different values of X, and using the Blatt and Weisskopf energy dependence (BW). We found, as did the authors of Ref. 23, that the best fits are obtained for the energy dependence (ND) with no k^2 dependence in the denominator,

$$V_i(E) \propto k_i^{2l_i+1}/E.$$

TABLE XII. Data used for fits to SU_3 coupling constants. Reactions are indicated by N_R: 1. $N\pi \to N\pi$; 2. $N\bar{K} \to N\bar{K}$; 3. $N\bar{K} \to \Sigma\pi$; 4. $N\bar{K} \to \Lambda\pi$; 5. $N\pi \to \Sigma K$.

Multiplet	Mass (MeV)	Γ (MeV)	N_R	$\pm(x_e x_r)^{1/2}$
D_5 octet	$N(1670)$	140 ± 35	1	0.420 ± 0.030
	$\Sigma(1765)$	120 ± 38	2	0.436 ± 0.018
			3	0.074 ± 0.017
			4	-0.250 ± 0.025
	$\Lambda(1832)$	88 ± 10	2	0.090 ± 0.010
			3	-0.138 ± 0.018
F_5 octet	$N(1688)$	142 ± 37	1	0.620 ± 0.060
	$\Sigma(1925)$	146 ± 22	2	0.100 ± 0.030
			3	-0.137 ± 0.015
			4	-0.090 ± 0.020
	$\Lambda(1823)$	104 ± 16	2	0.639 ± 0.006
			3	-0.268 ± 0.027
F_7 decuplet	$\Delta(1950)$	190 ± 30	1	0.450 ± 0.060
			5	-0.090 ± 0.020
	$\Sigma(2034)$	118 ± 12	2	0.200 ± 0.080
			3	-0.086 ± 0.014
			4	0.200 ± 0.020
G_7 singlet	$\Lambda(2092)$	144 ± 26	2	0.290 ± 0.040
			3	0.096 ± 0.037

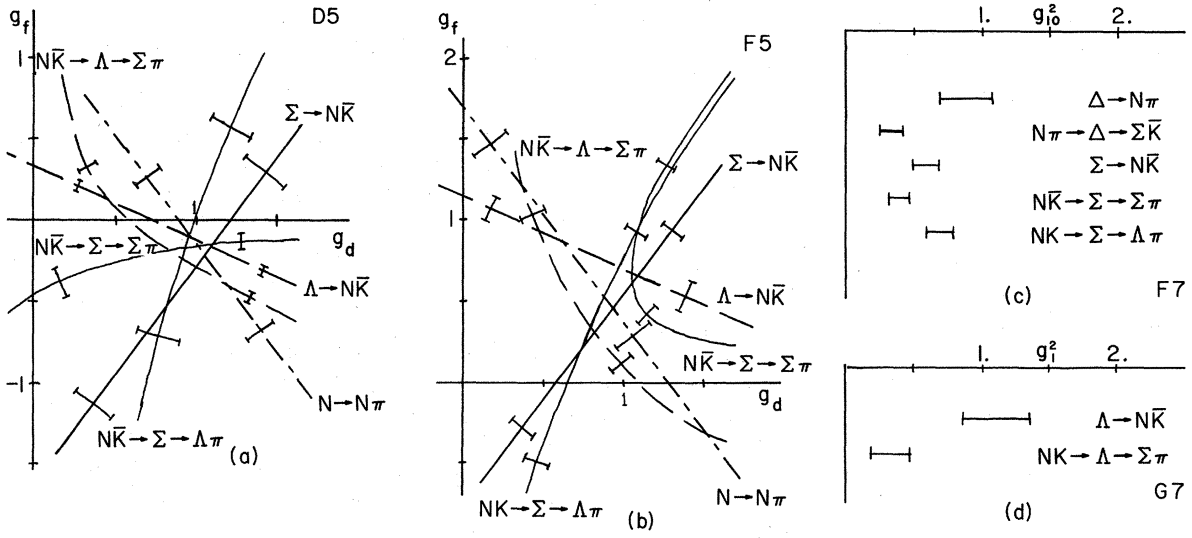

FIG. 5. SU_3 coupling constants calculated from the amplitudes for individual reactions assuming the GR energy dependence with $X=0.35$. The coupling constants are dimensionless; the scale factor was the nucleon mass. Elastic reactions are indicated only by the final-state channel. (a) D_5 octet. (b) F_5 octet. (c) F_7 decuplet. (d) G_7 singlet.

The variations in χ^2 for the various multiplets are shown in Fig. 6. We emphasize that the statistical significance is minimal since the errors in Table XII merely reflect the spread of values from different fits.

This last energy dependence is quite different from that used in our original partial-wave analysis; the growth of the partial and full widths is not moderated as in the GR and BW dependences. This procedure of letting the interaction radius go to zero (equivalently letting X^2 dominate the denominator) was first suggested for fitting the decay rates of the $\frac{3}{2}^+$ decuplet, based mainly on the distinction between widths observed in production processes and in partial-wave analyses.[25] These authors suggest that perhaps there is background under the resonance, ignored in the partial-wave analysis. To test this we performed two fits differing only in the energy dependence of the resonant couplings: In the first we used our standard dependence, the GR type with $X=0.35$; in the second we used $X=10$, which approximated the ND dependence. The results were not conclusive. The fits achieved probabilities of 43% and 17%, respectively; however, several waves in the former were in gross violation of the Wigner condition. We have observed this same phenomenon – high-probability solutions which violate causality – while fitting the data in limited energy ranges (see, for example, Ref. 1); and we have associated it with over-parametrization. In the present case the D_{13} wave was parametrized $R(0)+R(3)+P(6)$ in the notation of Table VII. Before carrying these tests further, therefore, we plan to extend the partial-wave anal-

TABLE XIII. SU_3 coupling constants from fits to data in Table VIII, assuming Glashow and Rosenfeld energy dependence with $X=0.35$ and the nucleon mass as scale factor.

	g_d	g_f	g^2
D_5	0.88	−0.14	
F_5	0.87	0.52	
F_7			0.49
G_7			0.51

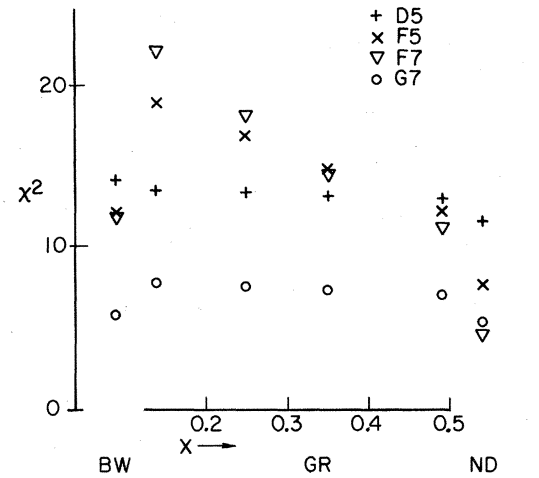

FIG. 6. Values of χ^2 for fits to SU_3 coupling constants for each multiplet. Three types of energy dependence were tried: the Blatt and Weisskopf form (BW) with an interaction radius of 1 F; the Glashow and Rosenfeld form (GR) with different values of the form-factor parameter X; and the "no denominator" form (ND): k^{2l+1}/E.

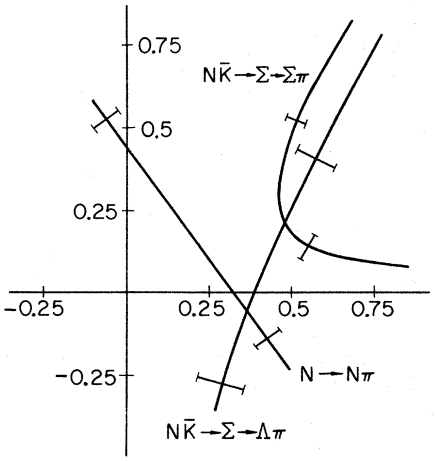

FIG. 7. SU_3 coupling constants for possible D_3 octet including our D_{13} resonance and the $N(2040)$. The GR energy dependence with $X=0.35$ is assumed.

ysis to a broader energy range. But since the energy dependence which best fits the data may not be the one which best agrees with SU_3 symmetry, it may be necessary to introduce symmetry breaking into the reduced couplings.

Finally we may make a tentative statement about the SU_3 classification of the new resonance in D_{13}. (Speculation about the last three resonances in Table XI would be premature.) The resonant nature of the D_{13} wave around 1.94 to 1.98 GeV has been seen in the $\Sigma\pi$ final state (this experiment and Ref. 10) and in the $\Lambda\pi$ final state (only in Ref. 10). In both final states the resonant amplitude t has the same relative sign. On the basis of this evidence, the resonance could not be associated with an SU_3 decuplet because the projection coefficients for the two final states have opposite sign. It may be associated, in an octet, with the D_3 nucleon resonance seen around 2.04 GeV. In Fig. 7 we have plotted the values of g_f, g_d obtained for these resonances by using the GR dependence with $X=0.35$ (analogous to Fig. 5). The information for $N(2040)$ was taken from Ref. 16: $\Gamma = 274 \pm 24$ MeV, $t_{N\pi} = 0.17 \pm 0.06$. For the Σ resonance our values are in good agreement with Ref. 10; we have used the following: $\Gamma = 208 \pm 22$ MeV, $t_{\Sigma\pi} = 0.10 \pm 0.02$, and $t_{\Lambda\pi} = 0.13 \pm 0.05$. We assigned a fairly large error to the last since it depends on only one observation. The results for g_f, g_d are certainly no less compatible than those from the D_5 and F_5 octets. The mean χ^2 contributions, though of limited significance, are indicative: 2.2 for the D_5, 2.9 for the F_5, and 2.8 for the D_3.

VI. SUMMARY

We have performed a partial-wave analysis of the reactions $K^-p \to \pi^\pm\Sigma^\mp$. We have here presented the data on which this analysis was based as well as the results of the analysis. The primary result is the confirmation of resonant structures in the F_{15} and D_{13} waves; these resonances are well within our energy range and are strongly supported by our data. We have looked at the D_5 and F_5 octets, F_7 decuplet, and G_7 singlet for possible SU_3 symmetry in the reduced coupling constants. We found that the energy dependence giving best agreement with SU_3 symmetry may not be the one which best fits the data, but were unable to test this conclusively. We found that the new D_{13} resonance is compatible with the D_3 nucleon resonance seen around 2.040 GeV.

---

*Work done under the auspices of the U. S. Atomic Energy Commission.

[1]Daniel F. Kane, Jr., Lawrence Radiation Laboratory Report No. UCRL-20676, 1971 (unpublished).

[2]Daniel F. Kane, Jr., Ph.D. thesis, Lawrence Radiation Laboratory Report No. UCRL-20682, 1971 (unpublished).

[3]R. Bell, Phys. Rev. Letters 19, 936 (1967).

[4]R. Armenteros *et al.*, Nucl. Phys. 38, 233 (1968).

[5]Herbert C. Albrecht *et al.*, Lawrence Radiation Laboratory Report No. UCRL-18528 Rev., 1968 (unpublished).

[6]H. S. White *et al.*, Lawrence Radiation Laboratory Report No. UCRL-9457, 1960 (unpublished).

[7]A. Berthon *et al.*, Nucl. Phys. B24, 417 (1970).

[8]I. Butterworth (Rutherford Laboratory) private communication, 1971.

[9](a) Frank T. Solmitz, Ann. Rev. Nucl. Sci. 14, 375 (1964). (b) These formulas for P and ΔP are not correct when cuts are made in the data (or events are missed due to imperceptible kinks). The correct formulas were given in Roger Odell Bangerter, Ph.D. thesis, Lawrence Radiation Laboratory Report No. UCRL-19244, 1969 (unpublished). We thank Professor R. D. Tripp for pointing this out. We have compared the results of these formulas with our previous results: Because of limited statistics the differences are neither significant nor systematic.

[10]Angela Barbaro-Galtieri, in *Hyperon Resonances-70*, edited by Earle C. Fowler (Moore, Durham, North Carolina, 1970), p. 173. We thank the author for giving us the Legendre coefficients prior to publication.

[11]R. D. Tripp, in *Strong Interactions*, International School of Physics "Enrico Fermi," Course 33, edited by L. W. Alvarez (Academic, New York, 1966), p. 70.

[12]C. Michael, in *Methods of Subnuclear Physics* (Gordon and Breach, New York, 1968), Vol. II, p. 31.

[13](a) W. C. Davidon, Argonne National Laboratory Report No. ANL-5990 Rev., 1957 (unpublished). (b) E. R. Beals, Program VARMIT write-up, Lawrence Radiation Laboratory Computer Library Note (unpublished).
[14]S. L. Glashow and A. H. Rosenfeld, Phys. Rev. Letters 10, 192 (1963).
[15]J. M. Blatt and V. F. Weisskopf, *Theoretical Nuclear Physics* (Wiley, New York, 1966), p. 389.
[16]For particle properties determined from many observations, we refer to the Review of Particle Properties for averaging or compatibility studies. Complete references to original literature are given in this compilation. We have used the following edition: Particle Data Group, Phys. Letters 33B, 1 (1970).
[17]We use the standard notation L, I, $2J$. The letters S, P, D, F, G refer to $L=0,1,2,3,4$, respectively.
[18]R. Armenteros *et al.*, Nucl. Phys. B18, 425 (1970).
[19]Wesley M. Smart, Phys. Rev. 169, 1330 (1968).
[20]R. L. Cool *et al.*, Phys. Rev. Letters 16, 1228 (1966).
[21]J. J. de Swart, Rev. Mod. Phys. 35, 916 (1963). In our calculations we have used the conventions and projection coefficients of Ref. 16.
[22](a) R. D. Tripp *et al.*, Nucl. Phys. B3, 10 (1967). (b) R. D. Tripp, in *Proceedings of the Fourteenth International Conference on High Energy Physics, Vienna, 1968,* edited by J. Prentki and J. Steinberger (CERN, Geneva, 1968), p. 173. (c) R. Levi-Setti, in *Proceedings of the Lund International Conference on Elementary Particles* (Berlingska, Lund, 1969), p. 341.
[23]D. E. Plane *et al.*, Nucl. Phys. B22, 93 (1970).
[24]G. E. Kalmus *et al.*, Phys. Rev. D 2, 1824 (1970).
[25]H. Pilkuhn and A. Swoboda, Lett. Nuovo Cimento 1, 854 (1969).